bacteria

MDPI

Article

The Emergence of the Slc11 Clade MCb_{gut}: A Parsimonious Hypothesis for the Dawn of Lactobacillales in the Gut of Early Vertebrates

Mathieu F. M. Cellier

Centre Armand-Frappier Santé Biotechnologie, Institut National de la Recherche Scientifique (INRS), Laval, QC H7V 1B7, Canada; mathieu.cellier@inrs.ca

Abstract: The Lactobacillales (LB) stand apart among bacterial orders, using manganese (Mn) instead of iron to support their growth and swiftly ferment complex foods while acidifying their environment. The present work investigates whether a shift in the use of Mn could mark the origin of LB. Transmembrane carriers of the ubiquitous Slc11 family play key roles in LB physiology by catalyzing proton-dependent Mn import. In prior studies, the Slc11 clade found in LB (MntH Cb, MCb) showed both remarkable structural plasticity and highly efficient Mn uptake, and another Slc11 clade, MCg1, demonstrated divergent evolution coinciding with emergence of bacterial genera (e.g., *Bordetella*, *Achromobacter*). Herein, the Slc11 clade MCb is subdivided in sister groups: MCb_{ie} and MCb_{gut}. MCb_{ie} derives directly from the Slc11 clade MCa, pointing an intermediate stage in the evolution of MCb_{gut}. MCb_{ie} predominates in marine Bacillaceae, is more conserved than MCb_{gut}, lacks the structural plasticity that typify MCb_{gut} carriers, and responds differently to identical mutagenesis. Exchanging MCb_{ie}/MCb_{gut} amino acid residues at sites that distinguish these clades showed conformation-dependent effects with both MCb_{ie} and MCb_{gut} templates, and the 3D location of the targeted sites in the carrier structure together suggests that the mechanism to open the inner gate, and release Mn into the cytoplasm, differs between MCb_{ie} and MCb_{gut}. Building on the established phylogeny for *Enterococcus* revealed that a pair of genes encoding MCb_{gut} was present in the common ancestor of LB, as MCb_{gu1} and MCb_{gu2} templates exhibited distinct structural dynamics properties. These data are discussed when examining whether MCb_{gut}^{+} LB could emerge in the upper gut of early vertebrates (ca. 540 mya), through genome contraction and evolution toward Mn-centrism, as they specialized as gastric aids favoring stomach establishment in jawed vertebrates through bi-directional communication with host nervous, endocrine and immune systems.

Keywords: lactic acid bacteria; proton-dependent Mn import; Slc11 carriers; AF2 modeling; conformational plasticity; in silico mutagenesis; phylogeny; evolution; vertebrates; stomach

Citation: Cellier, M.F.M. The Emergence of the Slc11 Clade MCb_{gut}: A Parsimonious Hypothesis for the Dawn of Lactobacillales in the Gut of Early Vertebrates. *Bacteria* **2024**, *3*, 223–255. https://doi.org/10.3390/bacteria3030016

Academic Editor: Bart C. Weimer

Received: 21 June 2024
Revised: 4 August 2024
Accepted: 9 August 2024
Published: 14 August 2024

1. Introduction

The Solute carrier 11 (Slc11) family of proton (H^+)-dependent importers of Mn^{2+} and/or Fe^{2+} belongs to the APC superfamily and adopts the tridimensional (3D) LeuT fold [1–3]. This fold consists of tandem repeats of five transmembrane helices that display inverted transmembrane topology. The repeats fold intertwined and coexist in alternate 3D configurations that are exchanged as the carrier molecule switches between two main states, either outward open (OO) or inward open (IO). The absence of sequence similarity between the two halves of the Slc11 carrier hydrophobic core implies asymmetric evolution, which could favor directional substrate transport, i.e., H^+-dependent import [4,5].

Molecular evolutionary genetic and structural analyses revealed that Slc11 synapomorphy functionally distinguishes this protein family from the rest of the APC superfamily [6]. Slc11 synapomorphy comprises 11 (quasi) invariant amino acid (aa) residues forming a 3D network that articulates Slc11 substrate-selective carrier conformational exchange between

the OO state and the IO state. The functional maintenance of this 3D network amid diverging Slc11 clades (e.g., bacterial MCb and MCg1) testifies to the resilience and evolvability of the molecular mechanism embedded through this synapomorphy in Slc11 architecture.

Moreover, the Slc11 mechanism of carrier coupling to the transmembrane protonmotive force (pmf), to catalyze cytoplasmic import of divalent metals such Mn and Fe (Me^{2+}), demonstrated stepwise evolution in the form of serial synapomorphies that distinguished groups of Slc11 homologs found either in prokaryotes (the proton-dependent Mn transporters, MntH) or in eukaryotes (the Natural resistance-associated macrophage proteins, Nramp, Table S1).

MntH synapomorphies demonstrate successive sets of coevolutionary rate-shifts that progressively edified an extended 'H^+-network' interacting with the pmf, from anaerobic bacteria (MntH B, before aerobiosis) to aerobic bacteria (MntH A) and to hyperthermophile TACK and Asgard Archaea (MntH H). This latter evolutionary intermediate likely shared a common ancestor with the first eukaryotic representative of the Slc11 family (Nramp precursor, [7]).

The Slc11 H^+-network further evolved in eukaryotes, during the transition from the first to last eukaryotic common ancestor (FECA to LECA), yielding two types of Nramp: prototype Nramp, mainly found in primitive eukaryotes, and archetype Nramp, predominant in multicellular organisms of both animal and vegetal realms (Figure 1A). Coupled with phagocytosis, archetype Nramp can restrict bacterial survival by depleting the acidified phagosomal milieu of Me^{2+}, such as Mn and Fe [8]. Arguably, the evolution of the Slc11 mechanism of carrier coupling to the pmf resulted in functional antagonism, yielding eukaryotic Nramp carriers that import Me^{2+} more efficiently than their bacterial counterparts (MntH).

However, both types of prototype *Nramp* genes (*pN-I* and *pN-II*, Table S1) were independently transferred horizontally towards bacteria. Therefore, bacterial MntH are polyphyletic [9], either of prokaryotic origin (MntH B, MntH A, MntH H) or of eukaryotic ancestry (MntH C). Alphafold (AF) [10]/Colabfold (CF) [11] 3D modeling of native MntH carriers of eukaryotic origin, from the sister clades MntH Cb (MCb) and MntH Cg1 (MCg1) Figure 1), coupled with the modeling of phylogeny-informed site-directed mutants, demonstrated paths of divergent evolution which affected both the carrier shape and functional plasticity [6].

A hallmark of MCb carriers is their conformational flexibility, and protein sequences from distinct clades (>80% sequence identity) yield 3D models representing discrete conformers. Regarding MCg, a mutation altering both the H^+-network in transmembrane helix 4 (h4) and carrier shape contributed to found MCg1 clade, and further divergent epistasis within this clade yielded an apparently functional neovariant, whose emergence coincided with novel bacterial genera (*Bordetella* and *Achromobacter*). This unexpected result suggested that, by analogy, the emergence of the MCb carrier might correspond as well with the rise of other bacterial genera.

Indeed, MCb is the only Slc11 type found in the order Lactobacillales (LB), and the majority of known MCbs are encoded by LB genomes. In contrast, the close relatives Bacillales may harbor either *mntH A*, *mntH Ca* or *mntH Cb* genes [7]. The extraordinary flexibility and functional plasticity of MntH Cb 3D models may relate to high carrier efficiency, able to support LB's *mntH*-dependent competitive exclusion of other organisms [12,13].

It is perhaps no coincidence that LB stand out as a bacterial order that relinquished heme-based metabolism to become Mn-centric microorganisms. As Mn excess can jeopardize iron-based metabolic functions, high efficiency Mn import seems particularly suited to cells notably lacking iron-cofactored enzymes for respiration, antioxidant defenses and the tricarboxylic acid cycle [14,15] and which rely on Mn instead of Fe for growth [12,16,17]. Based on the available data, it can therefore be hypothesized that the emergence of the MCb clade is concomitant to the dawn of LB.

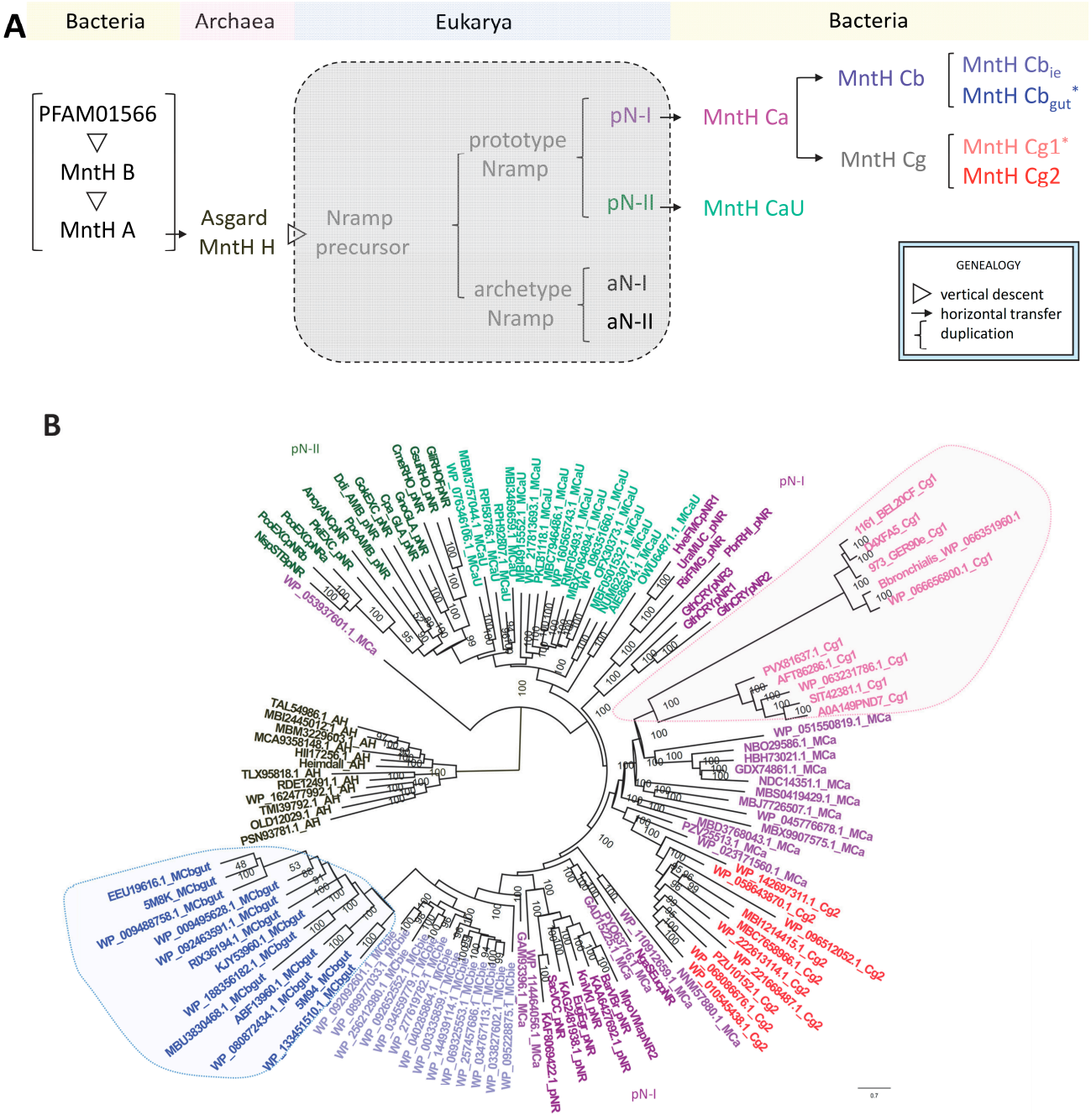

Figure 1. Phylogeny of bacterial Slc11 carriers of eukaryotic origin (MntH Ca (MCa), MCb, MCg and MCaU). (**A**) Recapitulation of the current knowledge on evolution of the Slc11 family (detailed in text) and proposition that MCb clade derived from MCa and comprises sister clusters, MCb$_{ie}$ and MCb$_{gut}$. Asterisks identify MC clades previously characterized as functionally divergent (highlighted in (**B**)). (**B**) Identification of MCb$_{ie}$ as possible evolutionary intermediate between MCa and MCb$_{gut}$ clades. The tree presented was rooted using MntH H seqs from TACK and Asgard archaea. Phylogenetic reconstruction used 395 PI sites, the substitution model EHO, ML estimate of a.a. state frequency, free rate model of variation among sites with 15 categories. The statistical significance of each node is indicated together with the scale (nb substitution per site). Phylogroups are highlighted with different colors and sequence ids. This phylogeny demonstrates partition of eukaryotic pN-I and pN-II parologs, and the common ancestries of pN-II and MCaU on one hand and pN-I and MCa, MCb, MCg on the other hand. MCb and MCg clades apparently derived from distinct MCas. The topology of MCb group suggests divergent evolutionary trajectories for MCb$_{ie}$ and MCb$_{gut}$, as previously observed in MCg1 subgroup [6].

The consensus on LB origin indicates they derived from a Bacillale ancestor through ~1/3 genome reduction and by adapting to some microaerated/anaerobic nutrient-rich environmental niche [14,15]. Given that LB are both notoriously proficient at predigesting (fermenting) complex food and common residents of animal gut [18,19], it seems plausible that LB could originate there. LB are demonstrated residents of the gut of various vertebrates (fish, reptiles, birds, and mammals) and a landmark study proposing the genus *Enteroccoccus* arose more than 425 million years ago (mya), as animals colonized land [20], suggests the LB common ancestor could have evolved earlier, during the Ediacaran–Cambrian transition for instance.

To test the hypothesis that the emergence of the (Slc11) MCb clade may coincide with LB origin, a sequence of possible evolutionary events linking MCa and MCb clades was established and their functional implications tested in silico using AF/CF 3D modeling. Several questions were addressed: Is there a group of MntH Cb seqs that display common properties identifying them as possible intermediates (hereby named MCb_{ie} for MCb environmental intermediate) between MntH Ca and the rest of the MCb clade (hereafter named MCb_{gut})? Do $MCb_{ie}{}^{+}$ microorganisms form a defined Bacillale taxon and/or share a common habitat? How do MCb_{ie} and MCb_{gut} in silico structural dynamics compare? Do they support a distinct mechanism of Mn import in LB? Does MCb_{gut} emergence predate the origin of Enterococci and what was the *mntH* Cb_{gut} gene complement of the common ancestor of LB?

The results presented define the Slc11 clades MCb_{ie} and MCb_{gut} which together form the phylogroup MCb. MCb_{ie} predominates in marine Bacillaceae and is closely related to both its ancestor clade, MCa, and the common precursor of MCb_{gut}. Regarding MCb_{gut}, it is in fact a pair of genes, encoding MCb_{gu1} and MCb_{gu2}, that typifies LB. The three MCb clades MCb_{ie}, MCb_{gu1} and MCb_{gu2} vary in their evolutionary conservation and conformational properties as the opening of the carrier inner gate apparently evolved in the transition from MCb_{ie} to MCb_{gut}. These data are discussed, relating the emergence of $MCb_{gut}{}^{+}$ LB and the development of the gastro-intestinal tract of early vertebrates.

2. In Silico Results

2.1. P. halotolerans A0A1I3CNB9 Identifies the Clade MCb_{ie}, Intermediate between MCa and MCb_{gut}

Prior work suggested that reevaluating the phylogenetic structure of the MCb clade may delineate a putative precursor lineage (MCb_{ie}) from LB's MCbs (MCb_{gut}). NCBI sequence wp_092092601.1 from the Carnobacteriaceae *Pisciglobus halotolerans* (Uniprot ID: A0A1I3CNB9), representing a cluster of sequences (seqs > 70% aa id), identified the most basal branching node of MCb and demonstrated relatively little specific divergence compared to the rest of the MCb clade [7]. Detailing the phylogenetic relationships of the A0A1I3CNB9 clade, i.e., MCb_{ie}, amid eukaryotic prototype Nramps and other bacterial MntH C clades (Figure 1B) confirmed both its basal position relative to the rest of MCb homologs, i.e., the MCb_{gut} clade, and the relative sequence conservation of its members.

MCb_{ie} conservation contrasts with the diversity of the MCa clade, which comprises both the closest known relatives of prototype Nramp-I (pN-I) and candidate precursors of both MCb and MCg clades [7]. The phylogenetic position of MCb_{ie} identifies an evolutionary intermediate between MCa and MCb_{gut} (Figures 1 and S1). MCb_{ie} clade topology shows two subsets (Figure S1A): a 'crown' formed by conserved sequences from core marine Bacillales (Bacillaceae, Paenibacillaceae) plus more divergent subsets from other (Lacto)bacillales spp. that exhibit relatively reduced genomes.

MCb_{ie} is most prevalent in Bacillaceae (45 seqs, 95% id cutoff, Figure S1A) and $MCb_{ie}{}^{+}$ genera represent about 10% of the Bacillaceae family (Figure S1B). MCb_{ie} phylogeny segregates several established genera of Bacillaceae, a pattern seemingly compatible with the vertical inheritance of *mntH* Cb_{ie}. Yet, both Bacillaceae and Planococcaceae encode predominantly the more ancestral MntH A (MA) protein, which contrasts with Paenibacillaceae wherein MntH Ca (MCa) predominates (205 seqs, 95% id cutoff). Neither

Listeriaceae [21–23] nor Carnobacteriaceae (LB) harbor any MA coding gene, and contrarily to Paenibacillaceae, MCb (MCb_{ie} or MCb_{gut}) is enriched in both of these families. In comparison, Lactobacillaceae possess exclusively MCb_{gut} (MCb_{gu1} and/or MCb_{gu2}, detailed in Section 2.6).

The topology of the MCb_{ie} 'crown' group shows clusters of seqs from Paenibacillaceae that diverge from clusters of seqs from Bacillaceae (Figure S1A). Moreover, only spp. of Paenibacillaceae (e.g., *Paenibacillus*: NZ_CP019717, NZ_CP020327 and *Brevibacillus*: CP048799, CP139435) were found harboring both genes encoding MCa and MCb_{ie}, including some *Paenibacillus* isolates wherein MCb_{ie} appears inactivated (NZ_CP019794, NZ_CP020557). Together with the large genome size of MCb_{ie}^{+} Paenibacillaceae spp., the data support that MCb_{ie} could originate in Bacillaceae and subsequently spread among Paenibacillaceae spp. Similarly, *mntH* Cb_{ie} gene transfers toward spp. showing genome erosion (e.g., Listeraceae and Carnobacteriaceae) may account for the relative divergence of their encoded MCb_{ie} proteins.

Phylogenomic analyses [24,25] support this interpretation, showing marine MCb_{ie}^{+} Bacillaceae, e.g., *Heyndrickxia* and *Lederbergia* genera, as more likely candidate precursors of LB than the MA^{+} *Bacillus* spp. (*B. subtilis* and *B. anthracis*, Figures 2 and S2). Staphylococcaceae and Listeriaceae are known as highly derived Bacillales families of Fe-dependent bacteria [26,27] and both lack MA encoding genes.

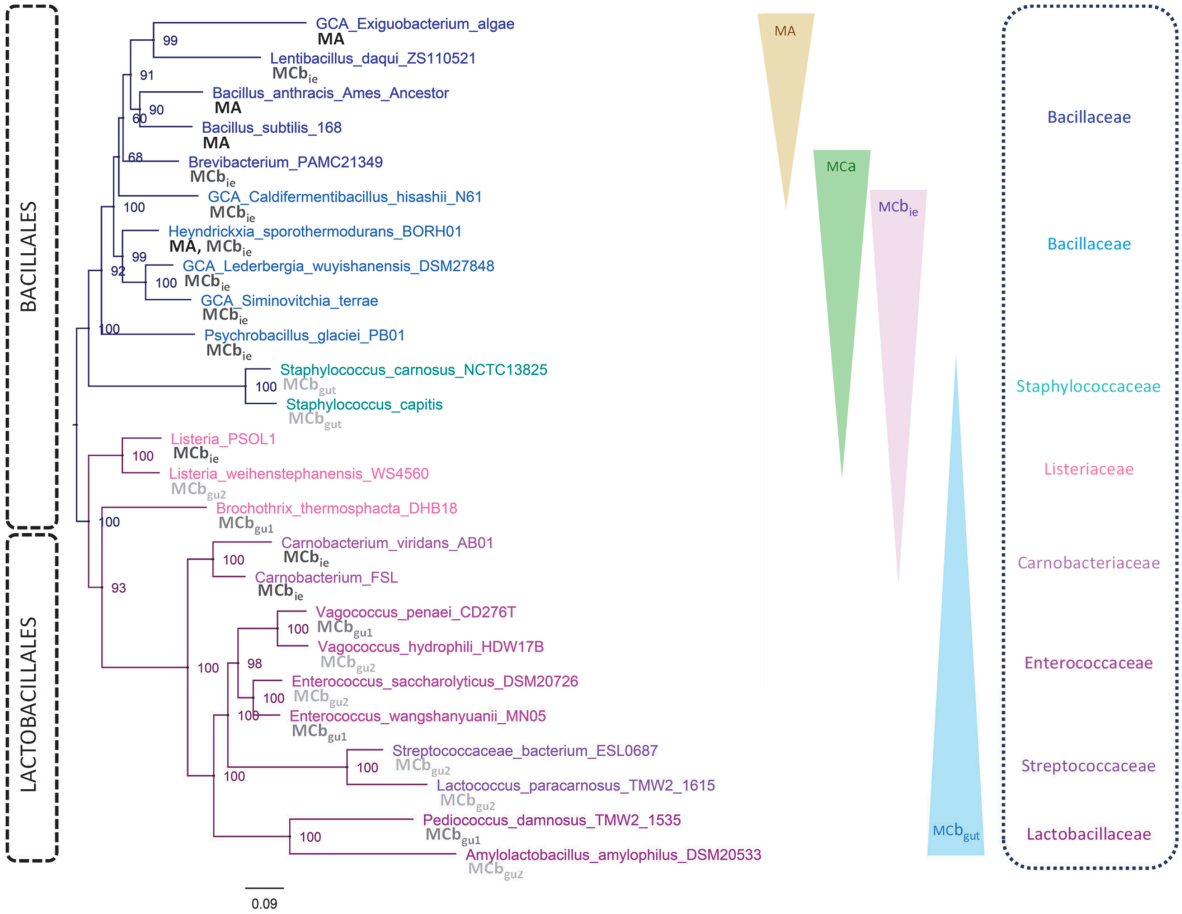

Figure 2. Bacillales and Lactobacillales phylogeny. Based on the VBCG pipeline [24] using select *mntH* encoding genomes plus IQ-Tree reanalysis (EX-EHO + R6) of the VBCG concatenated alignment. Species names are color-coded at family-level (indicated, right). *mntH*-encoded isotype is indicated per genome (bold). Appreciation of *mntH* gene flows according to the present hypothesis is schematized using colored arrowheads.

Altogether, the data presented clarify the emergence of the Slc11 clade MCb from its precursor MCa (itself derived from eukaryotic pN-I, Figure 1A). An intermediate step in this process produced the sister clades MCb_{ie} and MCb_{gut}, respectively, predominant in marine Bacillaceae, such as *Heyndrickxia* and *Lederbergia*, which are aerobic, and in anaerobic LB. These results provide molecular insight into the hypothetical evolutionary transition relating MA^+ Bacillales to $MCb_{gut}{}^+$ LB through a marine $MCb_{ie}{}^+$ Bacillaceae intermediate.

2.2. AF/CF 3D Modeling of Native MCb_{ie} and MCb_{gut} Carriers Differs Significantly

The multiple alignment of diverse sequences from the three groups MCa, MCb_{ie} and MCb_{gut} demonstrate 29 membranous sites that coevolved in the transition between MCa and MCb, i.e., coevolved mutations fixed in the common ancestor of MCb_{ie} and MCb_{gut} (Figure 3A,B). Also, sequence variations in extra membranous loops of the carrier molecule show several instances of selective conservation between MCa and MCb_{ie} vs. MCb_{gut} (e.g., l 4/5, l6/7, l7/8, l8/9 and l9/10, Figure S3), indicating that the common precursor of the MCb clade evolved directly from MCa.

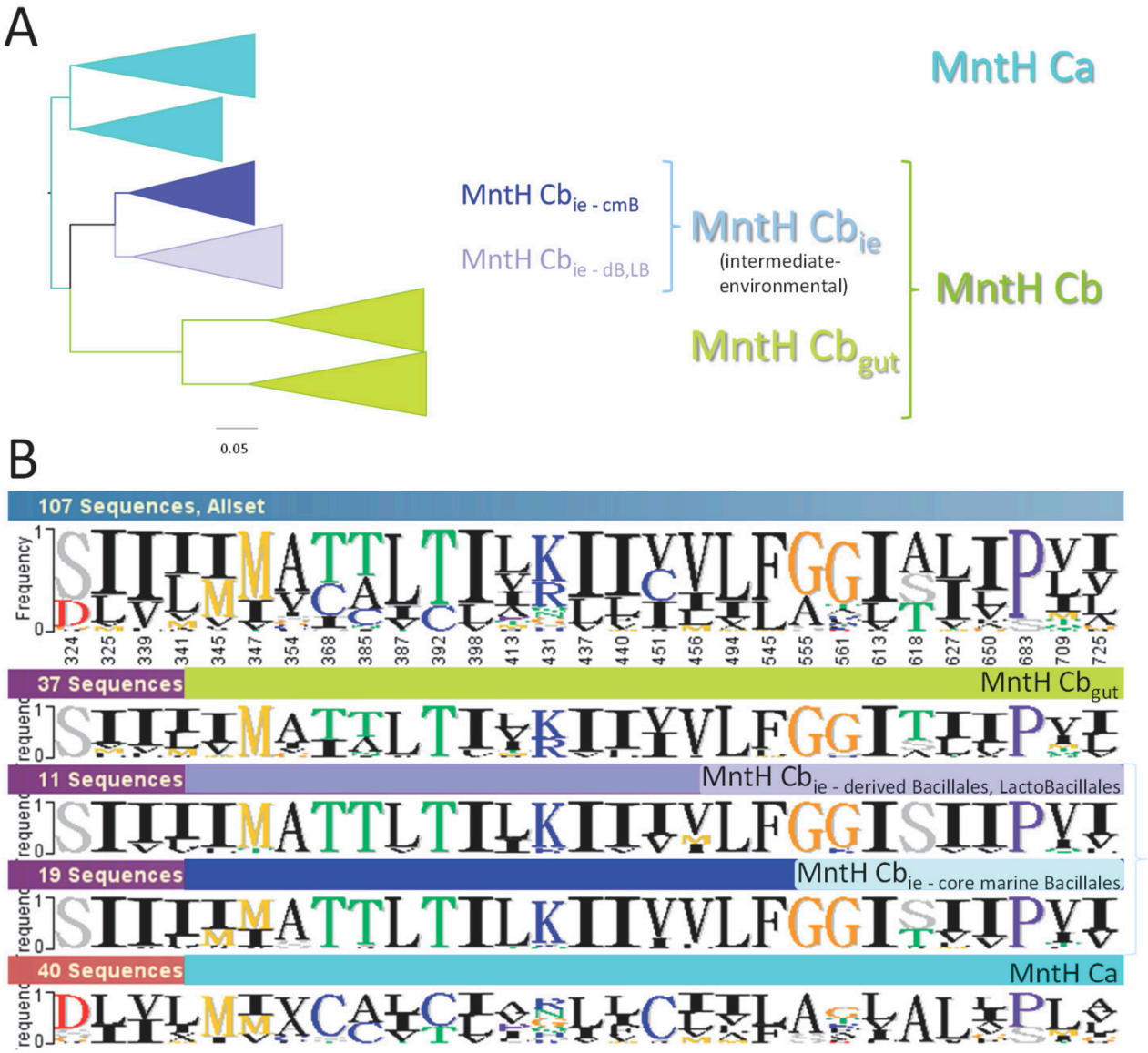

Figure 3. *Cont.*

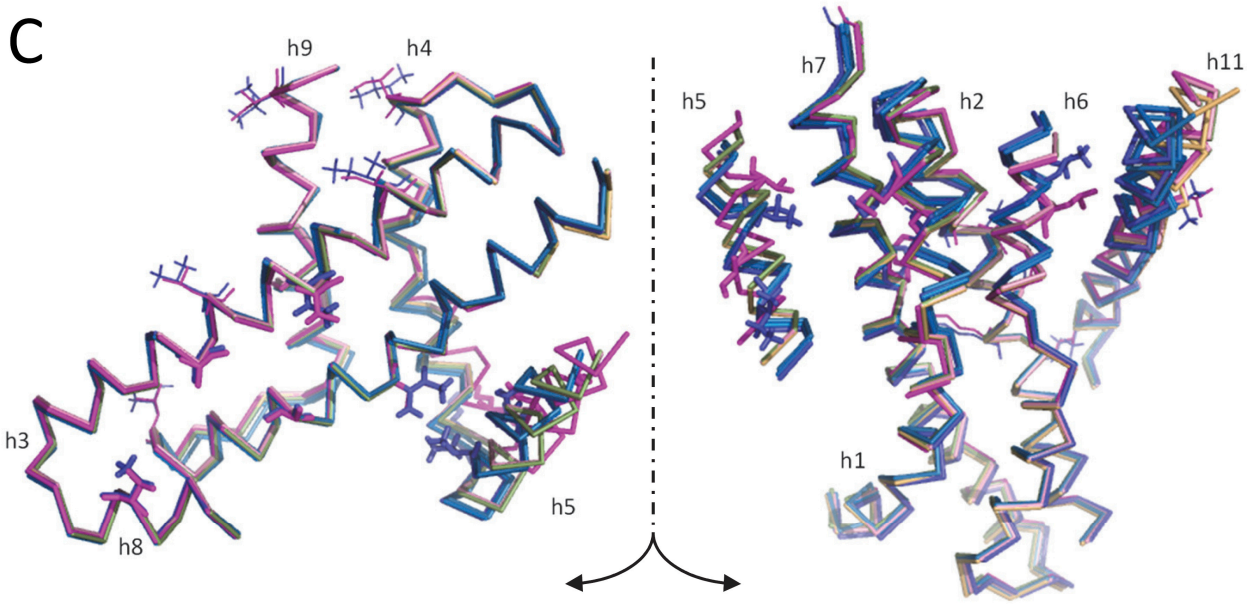

Figure 3. Structural evolution of MntH C in transition from MCa to MCb. (**A**) Similarity clusters highlight relationships between the groups of sequences analyzed in (**B**). (**B**) Phylo-mLogo display of the site-specific evolutionary rate-shifts that discriminate aligned MCb seqs (MCb_{ie} plus MCb_{gut}) from MCa seqs. (**C**) 3D location of the coevolutionary rate-shifts presented in (**B**). Superposed models (Cα ribbon) of previously characterized MCb conformers (AF-Q5HQ64, magenta, CF-Q5HQ64, light pink, CF-Q5HQ64_VY-YN-228T, dark blue; CF-A0A380H8T1, light green, CF-A0A380H8T1_VN223T, light blue; CF-WP_002459413, light orange, CF- WP_002459413_VN224T, marine blue) [6] allow visualizing site motion during carrier cycle. MCb architecture is presented after split of transmembrane helix 5 (h5) and opposite rotation of each half to display views from the center of the molecule. Transmembrane helices are numbered, and the extra membranous loops were omitted for clarity.

A 3D display of these 29 coevolved sites between MCa and MCb, on superposed MCb_{gut} models representing both the OO and IO states (cracked-open representation segregating half segments of helix 5 (h5), Figure 3C), shows accumulation along h5. The tilt of h5 modeled during MCb_{gut} carrier conformation switch was shown to mobilize separate communities of networked residues, involving one or the other half of h5, each contributing to open the inner gate of the carrier toward the cell interior [6]. The 29 (MCa/MCb) rate-shifted sites segregate in distinct areas involving either h5C, h7C, h1b, h2N, h6a and h11C (right panel) or h5N, h4C and h8N plus additional sites scattered across the 'hash module', which hosts a large part of the Slc11 H^+-network (left panel).

These data indicate that evolution of the precursor of the MCb clade directly from MCa involved a set of coevolved sites. These evolutionary coupled mutations, common to both MCb_{ie} and MCb_{gut}, may form a clade-specific (MCb) synapomorphy. Their accumulation in local areas of the 3D structure that involve one half or the other of h5, whose tilting during MCb_{gut} carrier cycle connects outer gate locking and inner gate opening [6], suggests these processes evolved in the transition from the MCa to MCb common ancestor.

The 3D modeling properties of MCb_{gut} templates differ from other MntH C clades, apparently due to their intrinsic carrier plasticity and the presence of flexible loops [6,7]. Based on the candidate MCb synapomorphy (Figure 3B,C), one could expect that AF2/CF models of native MCb_{ie} carriers would resemble known MCb_{gut} structures either modeled or solved. However, the 3D modeling of MCb_{ie} templates differed significantly (Figure 4).

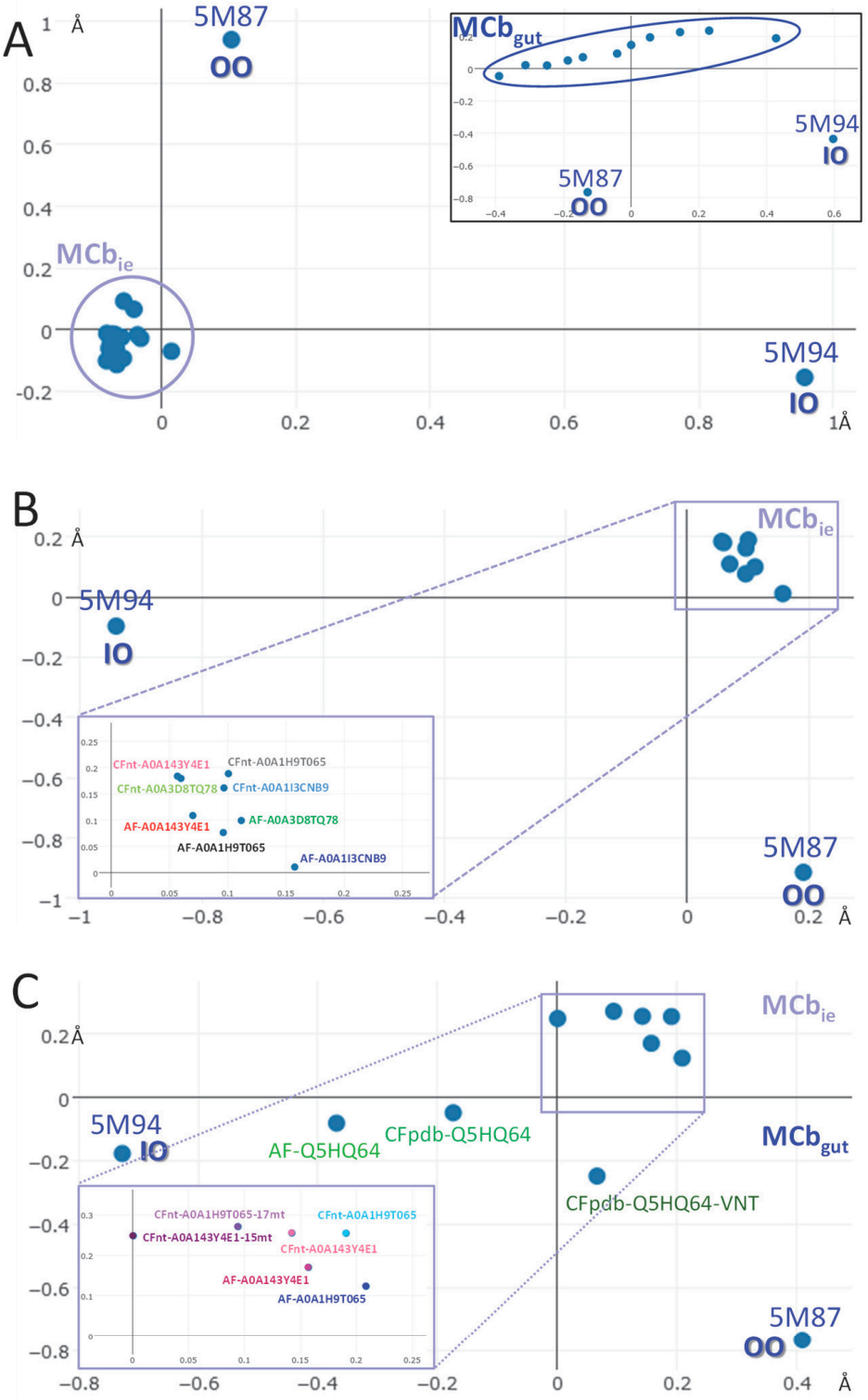

Figure 4. Three-dimensional modeling (AF2 or CF) demonstrates structural difference between MCb$_{ie}$ and MCb$_{gut}$. (**A**) Structural correspondence established by pairwise alignments of sampled AF2 models of MCb$_{ie}$ carriers and the solved reference structure of MCb$_{gut}$ carriers, either outward open (5M87, [28]) or inward open (5M94, [29]). Inset, array of native MCb$_{gut}$ models [6,7]. (**B**) Structural correspondence between AF2 and CFnt models of 4 MCb$_{ie}$ templates, details enlarged. (**C**) Impact of compound mutagenesis targeting a set of coevolved sites that discriminate MCb$_{ie}$ from MCb$_{gut}$ (presented in Figure 5A) on CFnt 3D modeling of select MCb$_{ie}$ templates. Additional reference models include MCb$_{gut}$ Q5HQ64 AF2 and CFpdb models (IO) and the Q5HQ64 VNT mutant (OO, CFpdb, [6]).

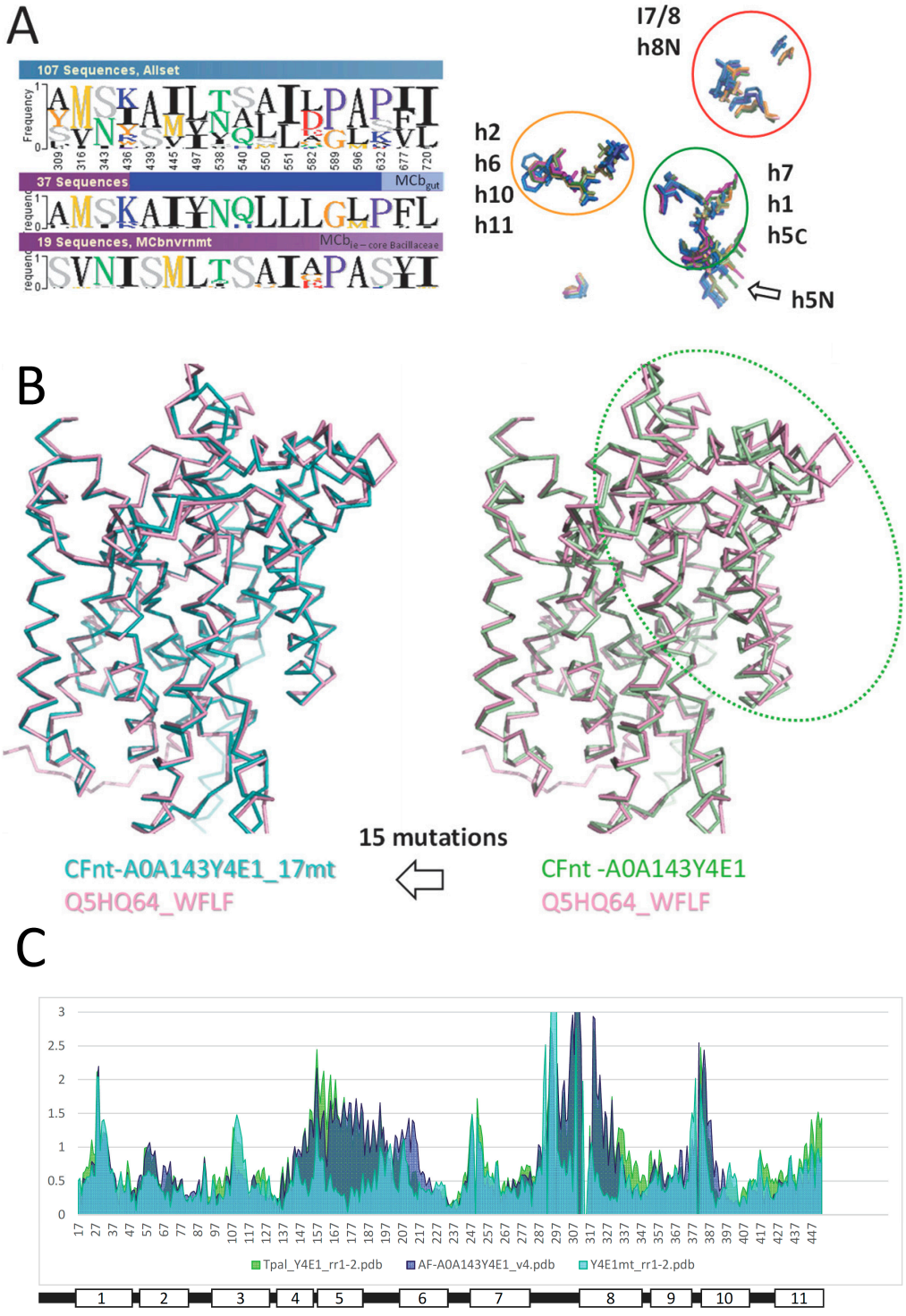

Figure 5. Structural reorganization of MCb$_{ie}$ A0A143Y4E1 after exchanging 15 residues that distinguish MCb$_{ie}$ and MCb$_{gut}$ clades. (**A**) 17 type ii evolutionary rate-shifts identified by comparing aligned representative seqs of MCb$_{ie}$ (core marine Bacillales) and MCb$_{gut}$ clades. Left panel, PhylomLogo display, right panel, 3D location on MCb$_{gut}$ models. (**B**) 3D superposition onto native MCb$_{gut}$ CFpdb model (Q5HQ64_WFLF, inward open) of MCb$_{ie}$ A0A143Y4E1 CFnt models predicted for the native (right) and compound mutant (A0A143Y4E1_15mt, left) templates. The dotted line shows local deviation between the structures compared. (**C**) Per residue root mean square deviation (pRMSD) from MCb$_{gut}$ inward open predicted structure (Q5HQ64_WFLF, CFpdb) of models obtained for MCb$_{ie}$ A0A143Y4E1 templates either native (AF2, CFnt) or after compound mutagenesis (A0A143Y4E1_15mt, CFnt, mutations detailed in Table S2).

The 3D correspondence of available Uniprot/AF2 MCb_{ie} models showed very similar predicted structures that did not clearly segregate with either the OO state or the IO state of solved structures of MCb_{gut} homologs (Figure 4A). This result contrasts with the array of functional conformers that AF2 predicted using MCb_{gut} sequences (Figure 4A, inset).

Examining the models obtained for four representative MCb_{ie} templates (~70% pairwise aa id) shows they do not represent clearly distinct OO or IO candidate conformers (Figure 4B), and their sequence relationships (cf Figure 1B, i.e., between WP_256212980.1 (NCBI proxy for Uniprot A0A143Y4E1), WP_092092601.1 (A0A1I3CNB9), WP_092652552.1 (A0A1H9T065) and WP_277619782.1 (proxy for A0A3D8TQ78)) suggests MCb_{ie} phylogeny does not influence AF2 or CFnt predictions. The two sequences that produced similar CFnt models, apparently closer to the MCb_{gut} IO state, were selected for further analysis (A0A143Y4E1 and A0A1H9T065, both from Carnobacteriaceae spp., *Trichococcus palustris* and *Isobaculum melis*, respectively).

The topology of the MCb clade (MCb_{ie} and MCb_{gut}) resembles the previously characterized MCg1 clade ([6] and Figure 1B): both subdivide in sister groups that differ in their relative extent of divergence. For the MCg1 clade, this situation was correlated with (i) founding mutations that introduced intrinsic structural constraints and (ii) reversion to a less constrained model structure as a result of extensive epistatic divergence.

Regarding MCb_{gut}, divergence from the MCb common ancestor produced remarkably flexible and intrinsically dynamic structures, whose predicted conformations reflected phylogenetic diversity (Figure 4A, inset). In contrast, the 3D models obtained using relatively diverse MCb_{ie} seem structurally constrained (Figure 4B), suggesting that MCb_{gut} could evolve out of epistatic divergence from (its common ancestor with) MCb_{ie}.

2.3. Evolution of MCb Carrier Cycling between MCb_{ie} and MCb_{gut}

To examine this, the possible functional evolution between MCb_{ie} and MCb_{gut} was investigated by comparing the AF/CF 3D modeling of native and mutant templates targeted at sites that underwent coevolutionary rate-shifts in the transition from MCb_{ie} to MCb_{gut} (putative MCb_{gut} synapomorphy). Meaning, 15 or 16 mutations that distinguish MCb_{gut} from MCb_{ie} were cointroduced into the sequences A0A143Y4E1 and A0A1H9T065, respectively (71.5% aa id, Figures 4C and 5A and Table S2). This approach aimed at testing the impact on the MCb_{ie} predicted structure of 17 comutations that typify instead the MCb_{gut} clade.

As a result, the CFnt modeling of the compound mutant A0A143Y4E1_15mt (Table S2) predicted a structure closer to the IO state of MCb_{gut} (Figure 4C). This suggested MCb_{gut} synapomorphy may signify functional determinants, as the corresponding residues map to 3D areas either partially overlapping with MCb synapomorphy (Figure 5A and Figure 3B,C, respectively) or specific to MCb_{gut} (e.g., l 7/8). In addition, while the native MCb_{ie} A0A143Y4E1 CFnt model cannot fully superimpose onto the MCb_{gut} IO CFpdb model (Q5HQ64_WFLF, [6]), the predicted structure for the compound mutant A0A143Y4E1_15mt does so almost perfectly (Figure 5B).

These data suggest that a select portion of MCb_{gut} carrier, which contributes to inner gate opening [6], was rearranged compared to MCb_{ie}. Per residue root mean square deviation (pRMSD) from the MCb_{gut} IO CFpdb model (Q5HQ64_WFLF) shows the segments rearranged in the MCb_{ie} compound mutant include l1/2 & h2, h4-h6, l 7/8 & h8, and l 9/10 & h10 (Figure 5C). These structural rearrangements extend beyond the areas targeted for mutagenesis (Figure 5A), implying the targeted sites may directly mediate MCb carrier conformation change.

Investigating this further, the reciprocal mutational approach was applied to MCb_{gut} homologs from distinct clades (>80% aa id) that produce discrete native conformers, either OO or IO or in between ([6] and Figure 6A), to determine how MCb_{ie}-specifying residues affect the MCb_{gut} predicted structure.

This yielded two types of results: (i) for templates whose predicted native conformers adopt the IO state, the 17 mutations introduced resulted in the prediction of OO conformers,

a result similar to that obtained by targeting instead five sites of Slc11 synapomorphy ([6] and Figure 6A,B); (ii) considering templates whose predicted native conformers adopt the OO state or in-between state, identical compound mutagenesis had comparatively little or no effect.

The conformational effects of the reciprocal mutageneses performed were both asymmetric and specific, favoring an MCb_{gut}-like IO state for the MCb_{ie} A0A143Y4E1_15mt mutant while triggering MCb_{gut} conformation switch from the IO state to the OO state but showing marginal effects on alternate MCb_{gut} carrier conformational states (OO and in between). Together these results demonstrate the functional impact of exchanging a set of coevolved residues that distinguish MCb_{gut} from MCb_{ie}, showing a conformation-dependent effect on MCb_{gut} carrier 3D modeling.

A

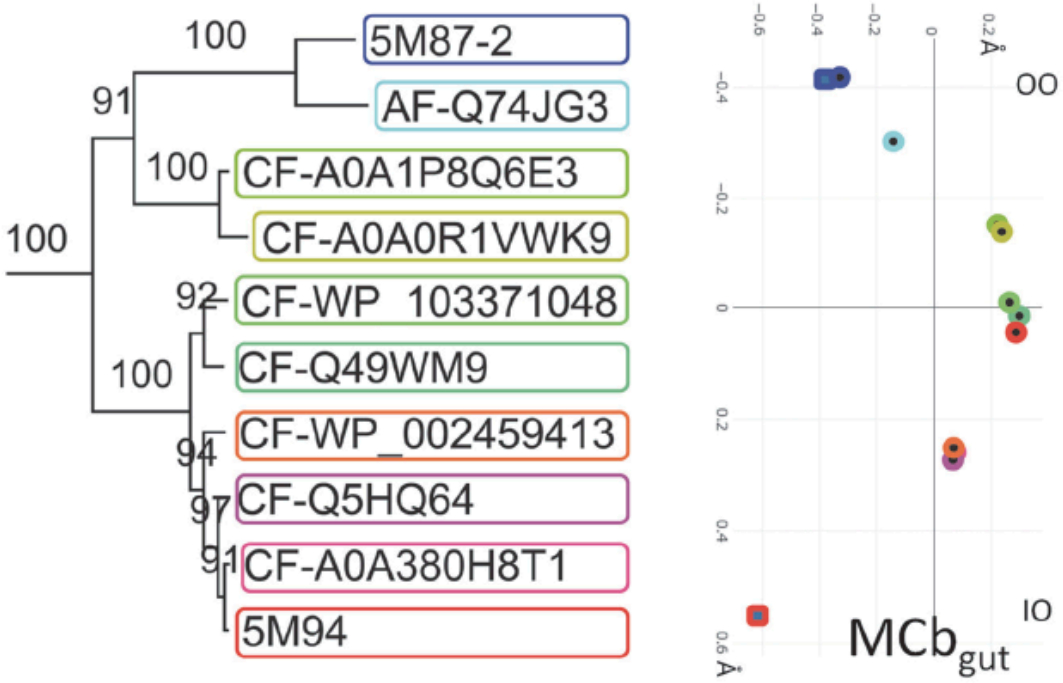

B

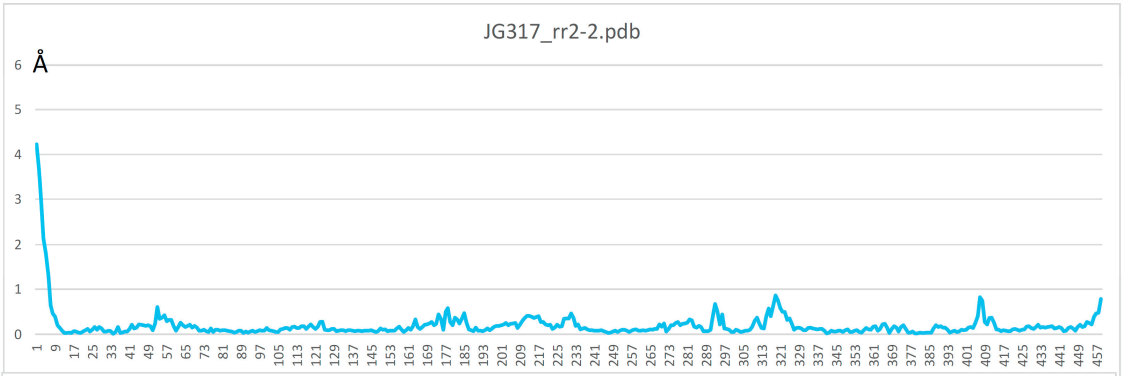

Figure 6. *Cont.*

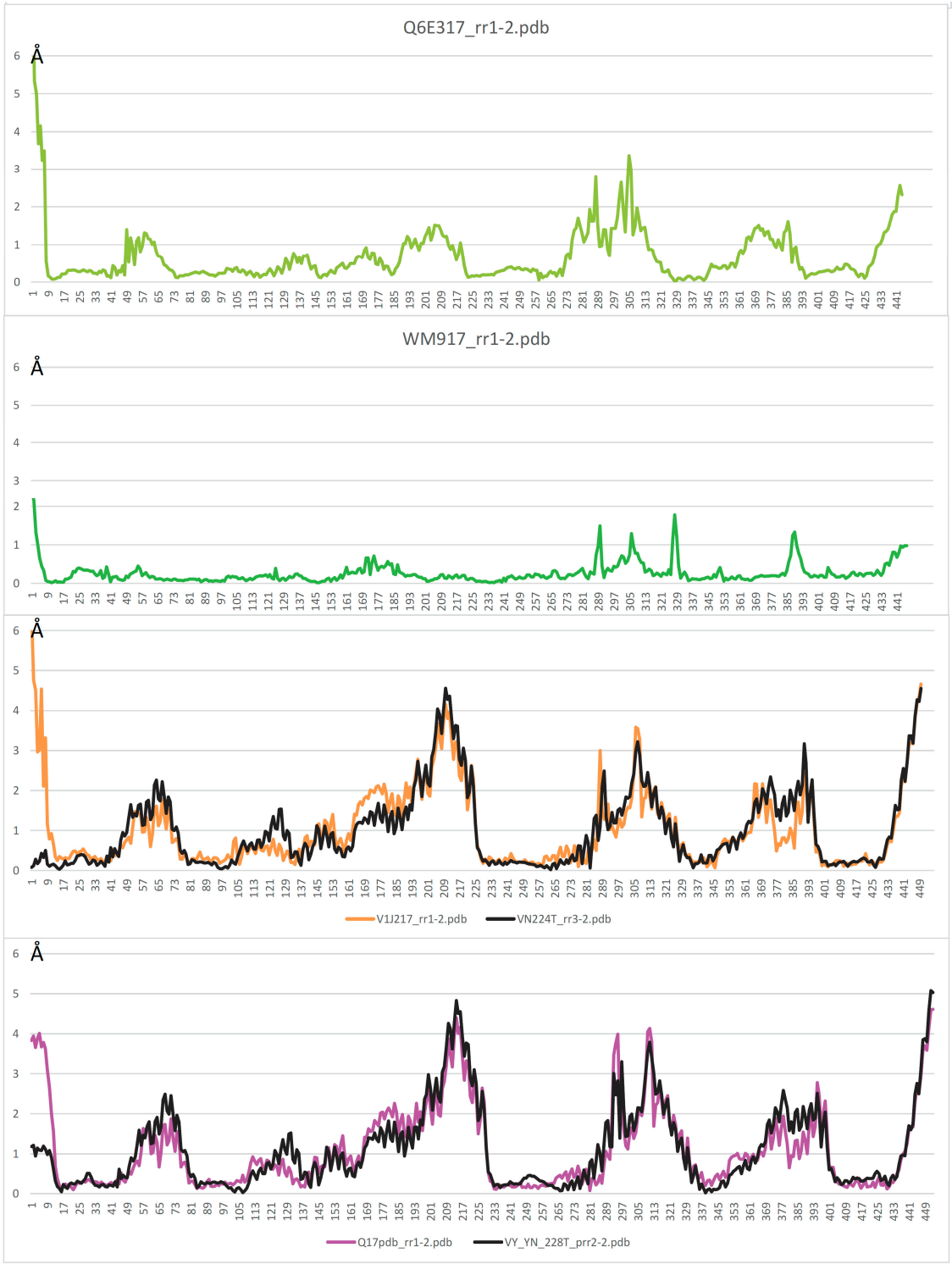

Figure 6. Conformation-dependent impact on MCb_{gut} CFpdb modeling of substituting 17 residues that discriminate MCb_{ie} and MCb_{gut} (reciprocal mutagenesis cf Figure 5 and Table S2). (**A**) MCb_{gut} phylogeny was previously shown to influence the conformers modeled by CFpdb [6]. (**B**) Co-introduction of 17 mutations in select MCb_{gut} templates shows conformation-dependent effects. Native CFpdb models were used as reference to determine the pRMSD of each respective mutant model. From top to bottom: Q74JG3, A0A1P8Q6E3, Q49WM9, WP_002459413, Q5HQ64. The pRMSD of WP_002459413 VNT and Q5HQ64 VNT mutant models [6] is also shown to visualize the expected deviation when comparing inward open and outward open conformers.

2.4. Mutagenesis of Slc11 Synapomorphy Supports Functional Divergence of MCb_{gut} and MCb_{ie}

A comparative analysis of CF modeling sensitivity to mutagenesis targeting Slc11 synapomorphy has proven useful to decipher the functional evolution between MCb and MCg1 clades and within the MCg1 clade [6]. The introduction of the canonical VNT mutation (h6 VY, h3 YN, and h6 T) into templates from both clades resulted in the conversion of native IO conformers into OO mutant conformers. However, the respective sensitivity to either h3 YN and/or h6 VY $^{+}/_{-}$ h6 T mutations varied between clades.

Applying the VNT mutation to MCb_{ie} A0A143Y4E1 produced the expected CFnt modeling result, which predicted an OO conformer like the reference MCb_{gut} Q5HQ64-VNT [6], indicated by a comparable broad scale rearrangement (Figure 7A) and quasi-superimposable structures (Figure 7B). In contrast, none of native A0A143Y4E1 predicted structures (using CFnt or AF2) nor the CFnt model for A0A143Y4E1_15mt fitted alike the MCb_{gut} OO model conformer. Hence, mutating five sites of Slc11 synapomorphy induced a conformational response of MCb_{ie} A0A143Y4E1 like those observed before with the MCb_{gut} and MCg1 clades.

However, detailing the effect of h3 YN and/or h6 VY $^{+}/_{-}$ h6 T mutations showed that, unlike MCb_{gut}, MCb_{ie} A0A143Y4E1 predicted conformation was fully switched in response to the h3 YN mutation only (Figure 8A,B), as previously observed using MCg1 A0A149PND7 [6]. Yet, contrary to MCg1 A0A149PND7, additional mutations targeting potential suppressor sites of a YN-induced conformation switch had no impact on the modeling of A0A143Y4E1 YN (Figure 8C).

In addition, A0A143Y4E1_15mt modeling was insensitive to h3 YN mutagenesis and neither the A0A143Y4E1 YN, A0A143Y4E1_15mt YN nor A0A143Y4E1_15mt model were affected by adding two other h3 mutations (Figure 8D). Furthermore, reversing three coevolutionary rate-shifts that distinguish MCb_{gut} in l 7/8 (DPA sites #582, #589, #596, Figure 5A) restored a degree of conformational response to h3 YN mutagenesis, observed with the A0A143Y4E1_15mt DPAYN model, akin to the A0A143Y4E1 YN modeling response (Figure 8E).

These results indicate MCb_{ie} modeling operated the conformation switch toward the OO state in response to the Slc11 synapomorphy VNT mutation, as expected from prior modeling studies of MCb_{gut} and MCg1. But MCb_{ie} A0A143Y4E1 modeling displays unique sensitivity to h3 YN mutation, which is lost after introducing 15 evolutionary coupled mutations that specify the clade MCb_{gut}. These data support divergent structure/function relationships between MCb_{gut} and MCb_{ie} and suggest a conformational role for intervening loops that are distal from the Mn^{2+} binding site.

A

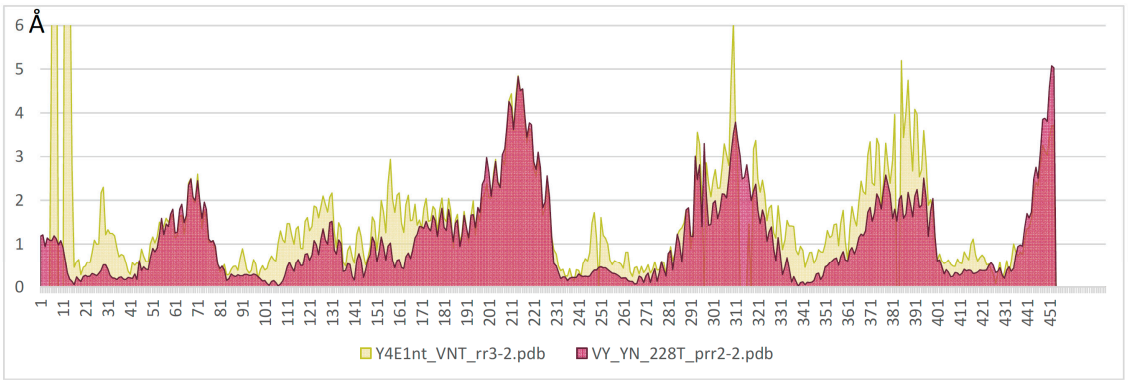

Figure 7. *Cont.*

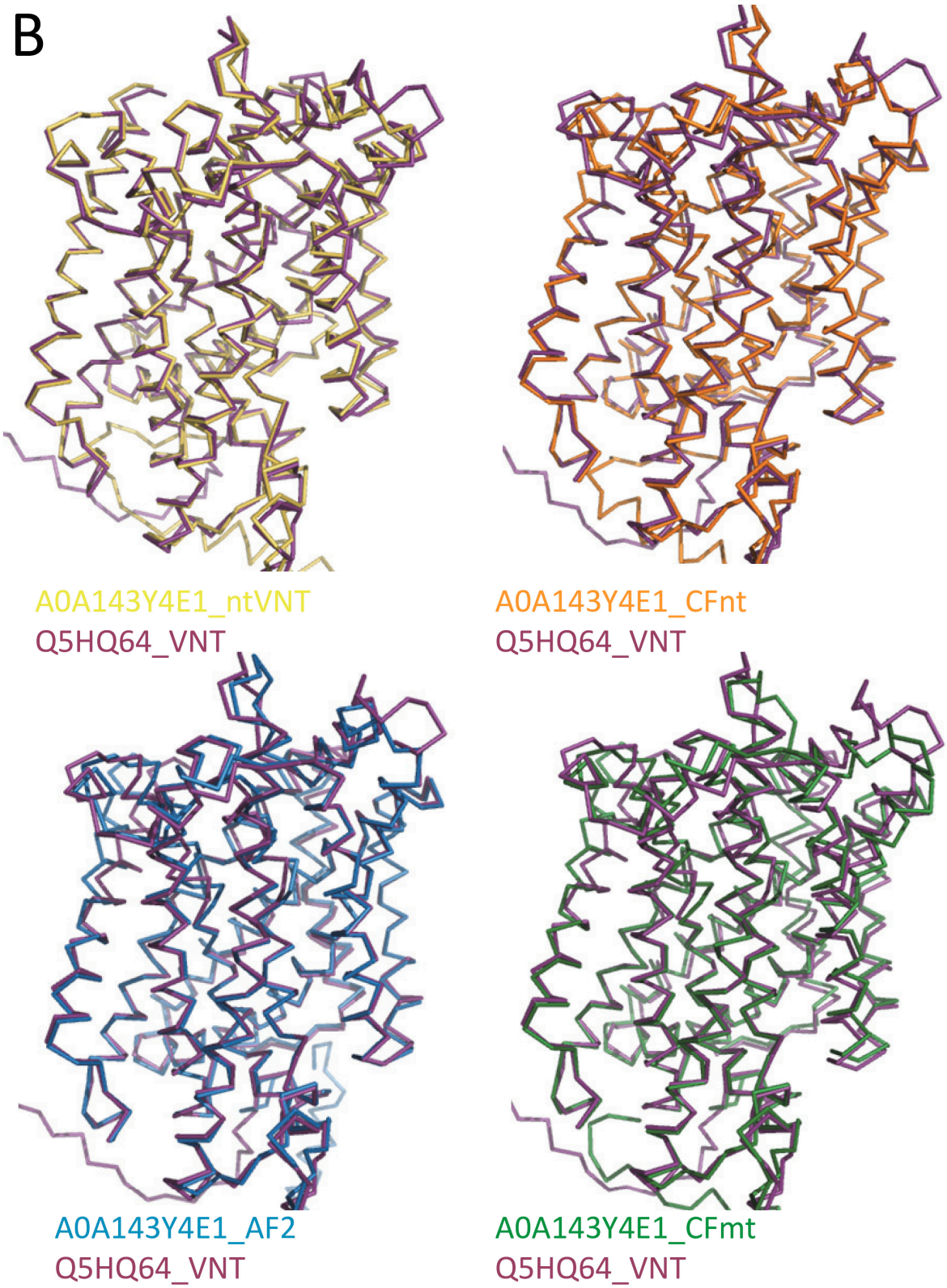

Figure 7. VNT compound mutagenesis of MCb_{ie} A0A143Y4E1 induces a conformational response like MCb_{gut} templates. (**A**) Identical VNT mutations (cf Table S2) result in similar rearrangements of the models predicted by CFnt (MCb_{ie} A0A143Y4E1) or CFpdb (MCb_{gut} Q5HQ64), indicated by pRMSD from MCb_{gut} Q5HQ64 native CFpdb model (inward open). (**B**) MCb_{ie} A0A143Y4E1 and MCb_{gut} Q5HQ64 VNT mutant 3D models are quasi-superimposable (top left).

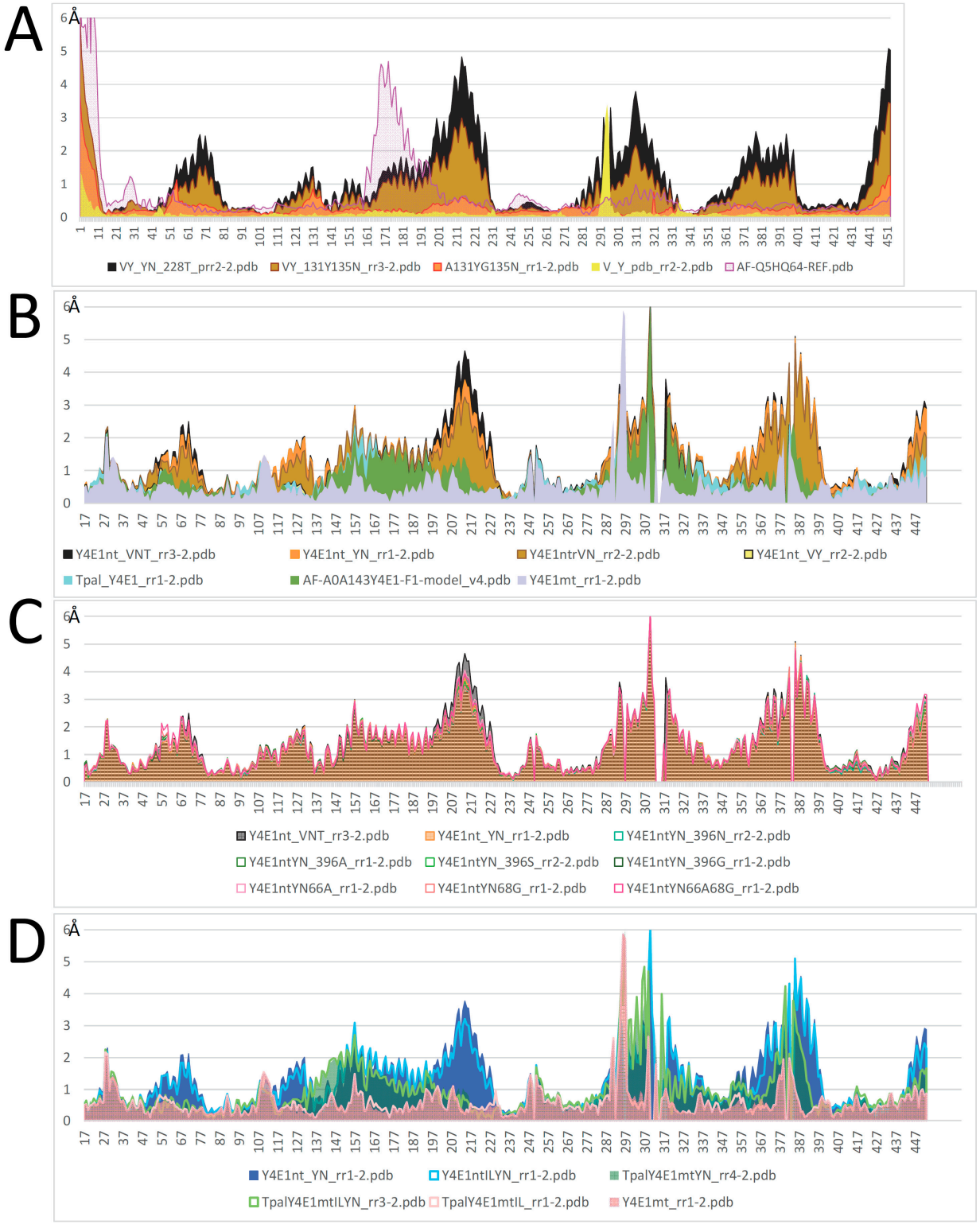

Figure 8. *Cont.*

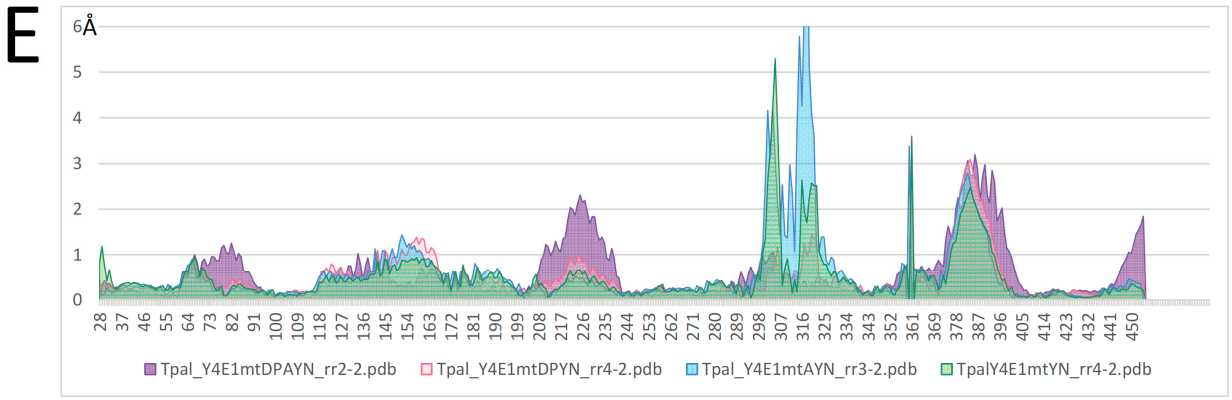

Figure 8. Distinct conformational response of MCb_{ie} A0A143Y4E1 to select mutations targeting sites of Slc11 synapomorphy. (**A**) Recap of the effect of VNT mutagenesis on MCb_{gut} Q5HQ64 (h3 A131YG135N, h6 A228T M231V H233Y, [6]) shown as pRMSD from Q5HQ64 native CFpdb model (inward open). (**B**) MCb_{ie} A0A143Y4E1 displays increased sensitivity to h3 mutation YN. (**C**) Modeling of MCb_{ie} A0A143Y4E1 YN-induced conformation change is unaltered by secondary mutations previously shown to suppress MCg1 A0A149PND7 YN-induced rearranged modeling [6]. (**D**) The impact of h3 YN mutation on MCb_{ie} A0A143Y4E1 CFnt modeling is lost in the compound mutant (A0A143Y4E1_15mt, cf Figure 5), and additional h3 mutations have no further effect. (**E**) Reverting 3 of the 15 targeted mutations co-assayed in MCb_{ie} A0A143Y4E1_15mt restores some modeling responsiveness to h3 mutation YN. The corresponding mutants are listed in Table S2.

2.5. Conformation-Dependent Impact of Mutations Targeting MCb l 7/8 and l 8/9

Reversing MCb_{ie}/MCb_{gut} rate-shifts in l 7/8 (DPA) was guided by observing that they map to a specific area of the MCb_{gut} structure (Figure 5A), i.e., not part of the evolutionary transition from MCa to MCb (Figure 3B,C) and polymorphic (Figure S3). And preserving this area as is in MCb_{ie} retained some conformational flexibility in the MCb_{ie} mutant A0A143Y4E1_15mt DPAYN (Figure 8E). Moreover, the functional importance of these DPA residues for MCb_{ie} conformational response to h3 YN mutagenesis is underscored by their conservation in the MCa clade (Figure S3, sites #582, #589, #596).

Along similar lines, mutation at site #632 (Figure 5A) in l 8/9 (Figure S3) was reevaluated. To mimic more precisely the MCb_{ie}/MCb_{gut} residue exchange vs. the MCb_{ie}/MCa exchange, the two sites #632 and #633 (cf Figure S3) were initially mutated in A0A143Y4E1_15mt (counted as one mutation). To verify whether this dual mutation also introduced a 3D constraint, it was reverted as well, either alone or combined to l 7/8 DPA reversion mutation (Figure 9A). In both instances, restoring MCb_{ie} native sequence in l 8/9 recovered some conformational flexibility. The modeling of the amended mutant A0A143Y4E1_15mt DPA-KP responded to YN-induced conformation exchange like native A0A143Y4E1 (Figure 9C). However, in the absence of the YN mutation, the amended mutant A0A143Y4E1_15mt DPA-KP deviated locally from the reference MCb_{gut} Q5HQ64 IO conformer (Figure 9B) and did not appear superimposable anymore (Figure 9C,D).

In sum, introducing 15 coevolutionary rate-shifts that distinguish MCb_{gut} from MCb_{ie} into MCb_{ie} recipient A0A143Y4E1 allows for the modeling of an IO conformer that is superimposable onto the MCb_{gut} reference IO conformer (A0A143Y4E1_15mt). Conversely, the reciprocal mutagenesis of MCb_{gut} members demonstrated native conformation-dependent effects, underscoring the functional significance of the targeted sites (cf Section 2.3).

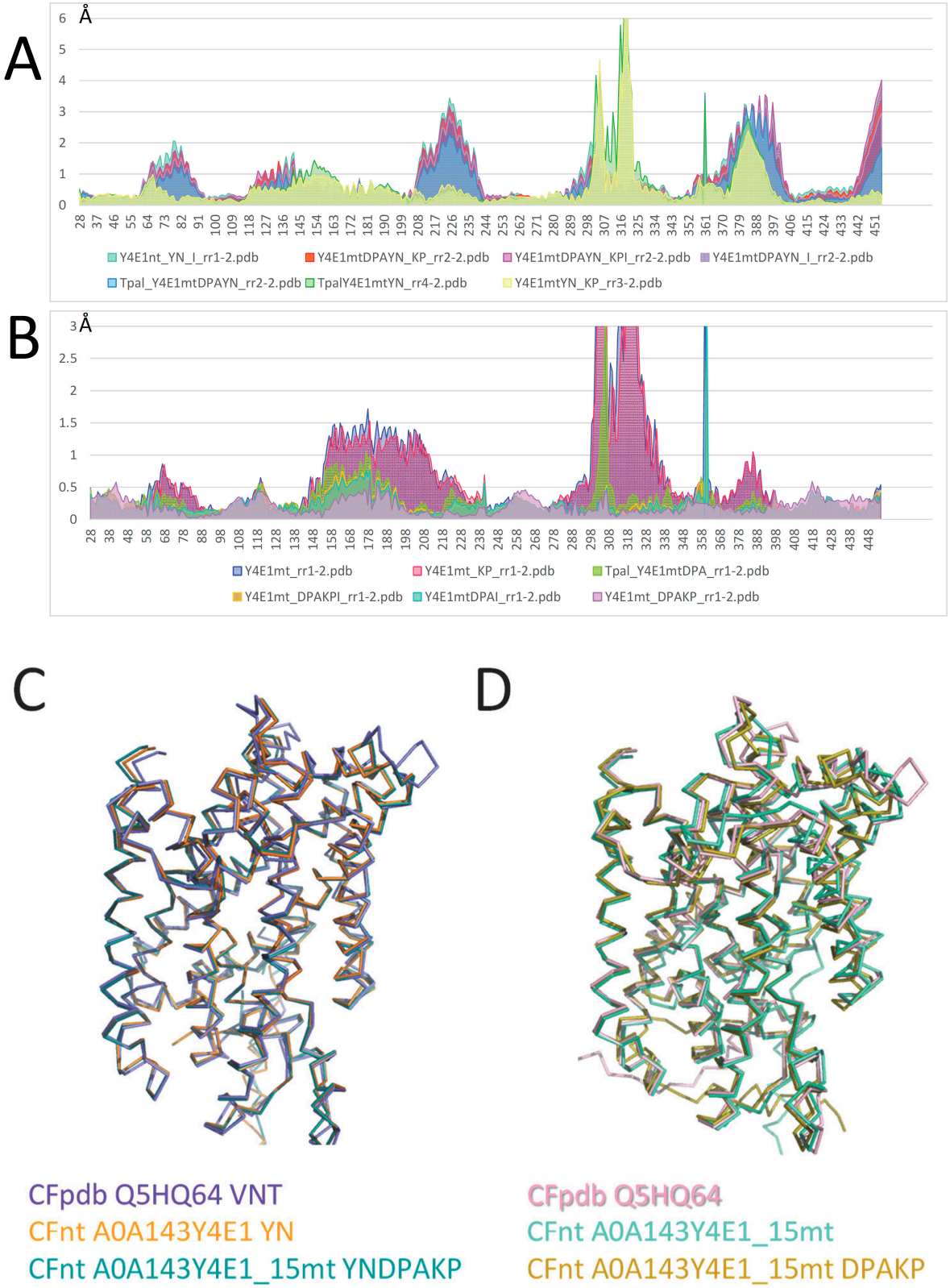

Figure 9. MCb_{ie} A0A143Y4E1 shows conformation-dependent responses to reversion of 5 of the 15 sites mutated in A0A143Y4E1_15mt. (**A**,**B**) pRMSD relative to native A0A143Y4E1 CFnt model. (**C**,**D**) Multiple 3D structure alignment using POSA. Reversion of 5 mutations from A0A143Y4E1_15mt (cf Table S2) has dual effects: it allows YN-induced conformation switch toward outward open state (**A**,**C**) but decreases 3D resemblance to MCb_{gut} Q5HQ64 inward open 3D model (**D**) by restoring instead similarity to the native MCb_{ie} A0A143Y4E1 model (**B**).

However, A0A143Y4E1_15mt lost 3D flexibility and responsiveness to the YN-induced conformation exchange from the IO state to the OO state. This impact was alleviated by reverting five of the mutations that targeted extramembranous loops distal from the substrate binding site (l 7/8 & l 8/9). Yet, these same reverted sites abrogated the 3D resemblance observed between the MCb_{ie} compound mutant and reference MCb_{gut} structure in the IO state. These five sites therefore demonstrate a conformation-dependent effect in the MCb_{ie} template A0A143Y4E1, and similar results were obtained using another MCb_{ie} template, A0A285P4W2 (from the Bacillaceae *Terribacillus aidingensis*, Figure S4).

To conclude, reciprocal mutations of coevolutionary rate-shifts that took place as MCb_{ie} and MCb_{gut} diverged exert distinct conformation-dependent effects on the 3D modeling of members of each clade. This implies the targeted sites contribute to the mechanism of MCb carrier cycling, but their respective role may differ within the MCb_{ie} or MCb_{gut} model structure. Together, these data relate MCb_{gut}-specific functional divergence to the IO state of the carrier, which seems consistent with a possible shift in Mn import capacity in LB.

2.6. MCb_{gut} Phylogeny Reveals a Pair of Distinct Carriers in the Common Ancestor of LB

To approximate a possible period for this functional transition, from marine $MCb_{ie}{}^{+}$ Bacillaceae toward $MCb_{gut}{}^{+}$ LB, MCb_{gut} phylogeny was further explored, first, among spp. of the Enterococcaceae family because its origin was dated (>425 million years ago [20]) and its structure comprises four clades, one of which diverged basally [30]. MCb_{gut} phylogeny is complex due to pervasive horizontal gene transfers [31] and multiple copies per genome (e.g., six in the *Levilactobacillus suantsaii* strain CBA3634 chromosome, NZ_CP059603.1). This may explain why the phylogenies of enterococcacal MCb_{gut} and Enterococci spp. vary (Figure S5). But the general topology of the tree and the profound dichotomy of the *Enterococcus* clade A vs. clades B-D were recovered, implying a significant phylogenetic signal encoded by MCb_{gut}. The separate grouping of MCb_{gut} seqs resulting from gene transfer to bacteria of different phyla, either enterobacterial or actinobacterial spp., indicates distinct events. The position of the Enterococcaceae *P. termitis* seq suggested it may demarcate two types of MCb_{gut}, meaning that perhaps the common ancestor of Enterococcaceae possessed a pair of distinct *mntH* Cb_{gut} genes.

To address this possibility, MCb_{gut} phylogeny was determined across the LB order using a set of representative seqs from each LB family (Figure 10). The results show the presence of two clusters of MCb_{gut}, labeled MCb_{gu1} and MCb_{gu2}, found both in Enterococcaceae and Lactobacillaceae. In addition, the data suggest two other clades could diverge independently from MCb_{gu2}.

The present tree thus supports the possible existence of two MCb_{gut} copies in the common ancestor of LB. Several spp. of Lactobacillaceae harbor both genes encoding MCb_{gu1} and MCb_{gu2} on their chromosome (e.g., NZ_LT854705.1, NZ_CP059603.1), implying perhaps some LB retained both genes since their origin.

The presence of both MCb_{gu1} and MCb_{gu2} in the common ancestor of LB suggests they are not functionally equivalent. To evaluate this proposal, three individual sequences from each type were subjected to AF/CF modeling using either native sequences or compound mutants. Native AF2 models showed that, both in Lactobacillaceae and Enterococcaceae, MCb_{gu1} and MCb_{gu2} yielded distinct conformers in the OO state (Figure 11A and Figure 11B, respectively). The MCb_{gu2} type appeared closer to the fully OO conformation and less structurally conserved among Enterococcaceae. The introduction of a set of (reciprocal) mutations corresponding to the MCb_{ie}/MCb_{gut} evolutionary transition (cf Section 2.3) confirmed it had little impact on the OO conformers of the MCb_{gu1} and MCb_{gu2} types. These data are in accordance with previous observations showing a strong phylogenetic component in the AF/CF modeling of MCb_{gut} [6].

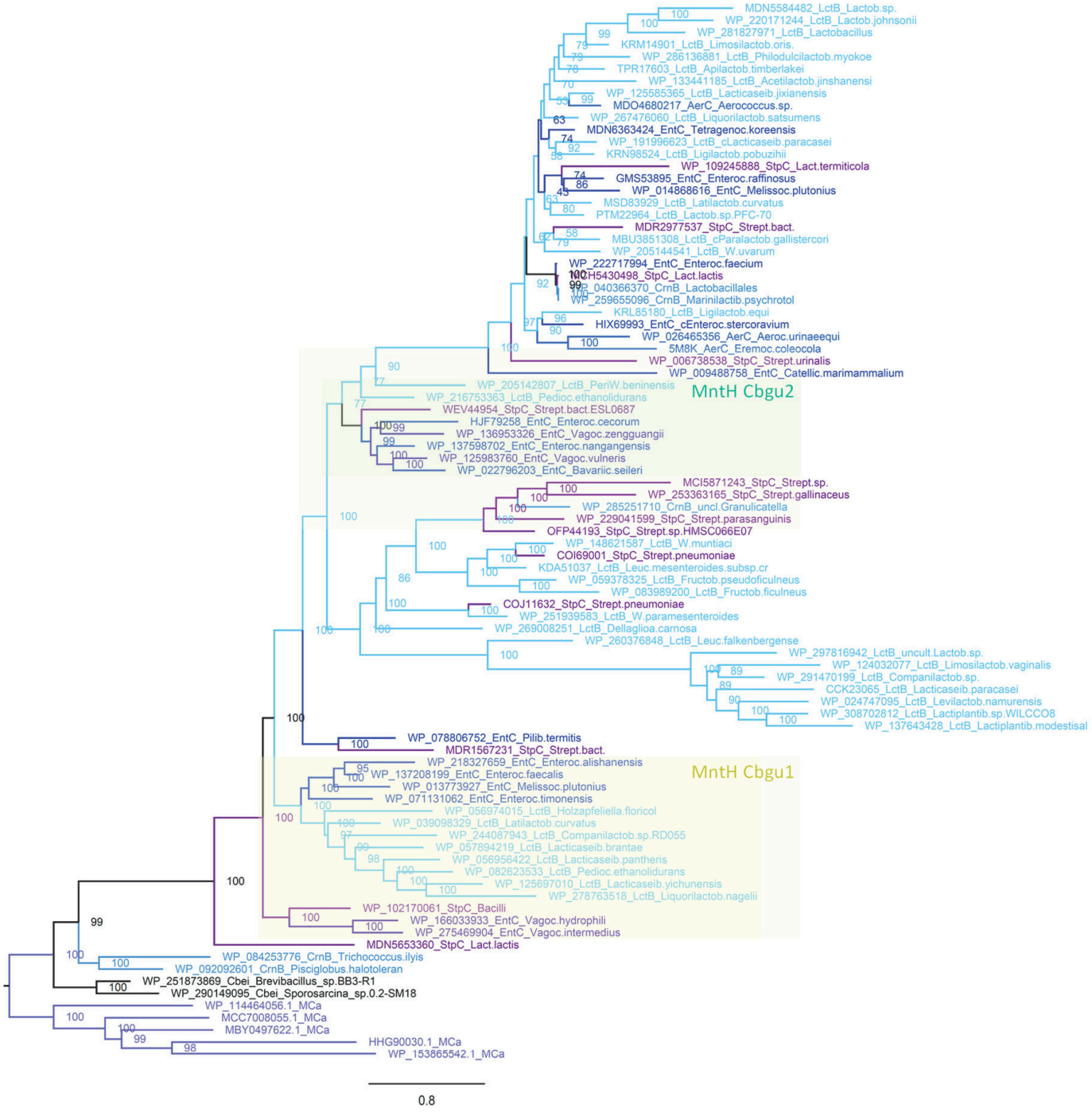

Figure 10. IQ-Tree phylogeny of MCb_{gut} among Lactobacillales (LB). Representative seqs from each LB family (Aerococcaceae, AerC, Lactobacillaceae, LctB, Streptococcaceae, StpC, Enterococcaceae, EntC, Carnobacteriaceae, CrnB) were analyzed using 5 MCa and 2 MCb_{ie} seqs as outgroup. The tree presented used 347 PI sites, the substitution model EX-EHO, ML estimate of a.a. state frequency, free rate model of variation among sites with 7 categories. The statistical significance of each node is indicated together with the scale (nb substitution per site). Two clusters of MCb_{gut} seqs, separated by *P. termitis* seq and that replicate the profound dichotomy observed by analyzing MCb_{gut} seqs from Enterococcaceae (Figure S5), are highlighted: MCb_{gu1} and MCb_{gu2}.

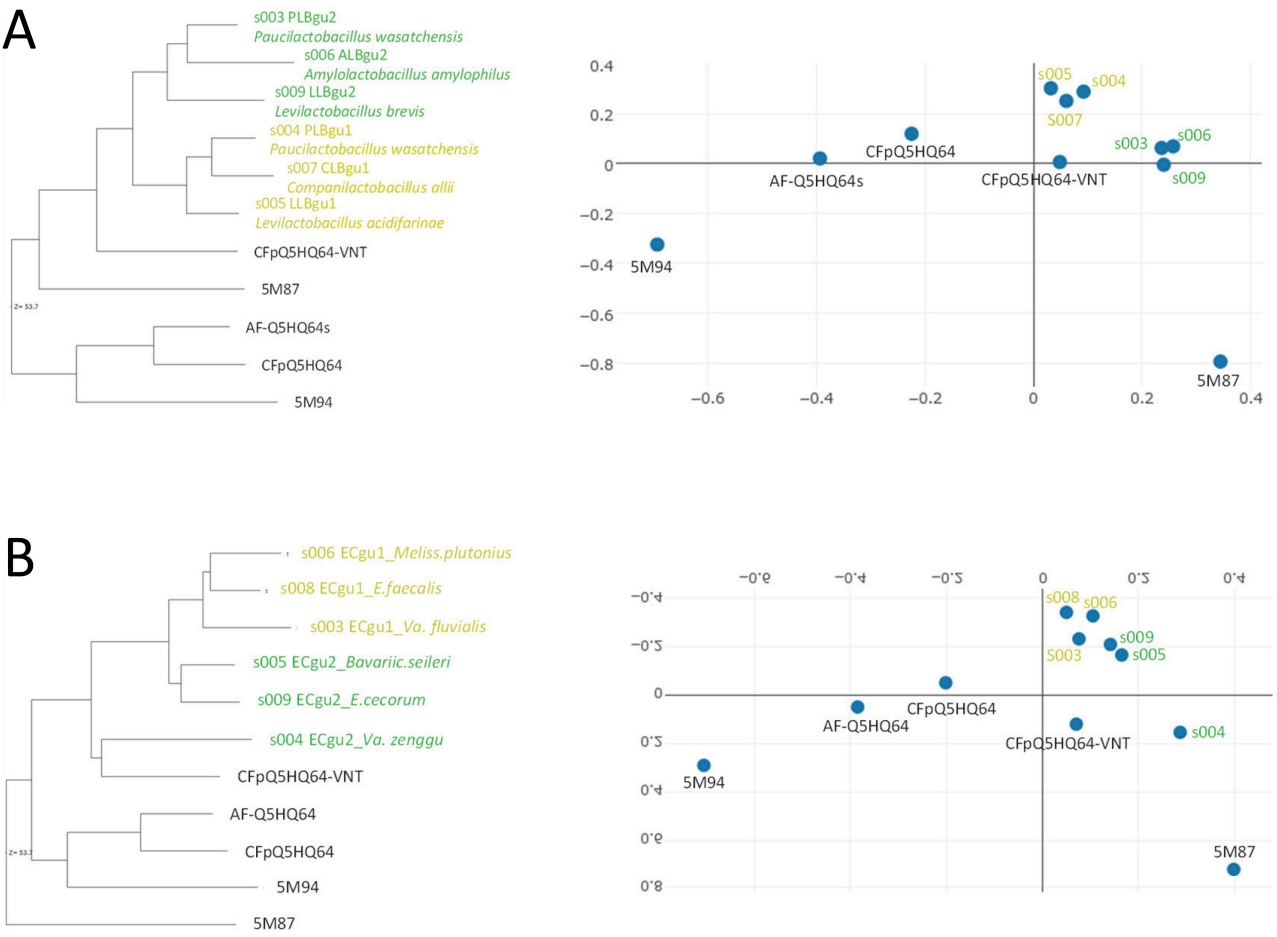

Figure 11. AF2 models distinct conformers for LB MCb_{gu1} and MCb_{gu2} templates. (**A**) Lactobacillaceae. (**B**) Enterococcaceae. Pairwise structural similarity was established with Dali all against all, using as 3D references the solved structures of MCb_{gut} in outward open state (5M87) and inward open state (5M94) as well as AF2 and CFpdb models of MCb_{gut} Q5HQ64 and CFpdb model of Q5HQ64 VNT. Similarity depicted using dendrogram (left) and 3D correspondence (right) representations.

To compare MCb_{gu1} and MCb_{gu2} structural dynamics a combination of mutations able to mimic the carrier forward transition, i.e., exchanging the OO state modeled by CF pdb using the native sequence for the IO state of a mutated carrier, was necessary. Along sites previously identified as conformationally active, either as part of Slc11 synapomorphy or contributing to inner gate opening, additional sites were targeted in helices 3, 4, 8 and 9, which together constitute the Slc11 carrier 'hash module' known to interact with the pmf [2,3]. All targeted sites are evolutionary conserved so that identical mutations were introduced among both the MCb_{gu1} and MCb_{gu2} templates (Table S2).

Introducing a series of 15 phylogenetically aware mutations into the *Paucilactobacillus wasatchensis* template PLB_{gu1} enabled us to model an IO conformer like the MCb_{gut} Q5HQ64 reference CF model (Figure 12A,C). Applying this combination of mutations to other MCb_{gu1} had a similar yet less pronounced effect, producing models more advanced toward, albeit not switched to, the IO state (Figures 12E and S6A,C). In comparison, the MCb_{gu2} mutant response appeared more sequence-specific with two templates (Ece_{gu2}, Lbr_{gu2}) progressing toward the IO state (Figures 12F and S6B,D).

To further distinguish the modeling properties of MCb_{gu1} and MCb_{gu2} templates, a set of discriminatory type ii evolutionary rate-shifts was targeted to perform reciprocal residue exchanges between MCb_{gu1} and MCb_{gu2} seqs (Figure 12D). Again, all three MCb_{gu1} behaved similarly and were modeled into more OO conformers, implying some antagonism between the two series of mutations tested altogether (Figures 12G and S6E). Reciprocal mutagenesis had distinct effects on MCb_{gu2} templates, which appeared either unchanged or further progressing toward the IO state (Figures 12H and S6F).

Lastly, evolutionary conservation among representative sets of MCb_{gu1} and MCb_{gu2} seqs suggests these clades experienced distinct selective pressures (Figures 12I,J and S7).

From these results, it is concluded that MCb_{gut} phylogeny replicates the evolutionary dichotomy previously established among *Enteroccoccus* spp. It appeared the common ancestor of LB likely possessed a pair of genes encoding seemingly distinct types of MCb_{gut}. The transition from marine Bacillaceae MCb_{ie} toward LB's MCb_{gut} could proceed sequentially with the functional evolution of a substrate-dependent step, such as inner gate opening, followed by gene copying and a separate evolution of distinct carriers.

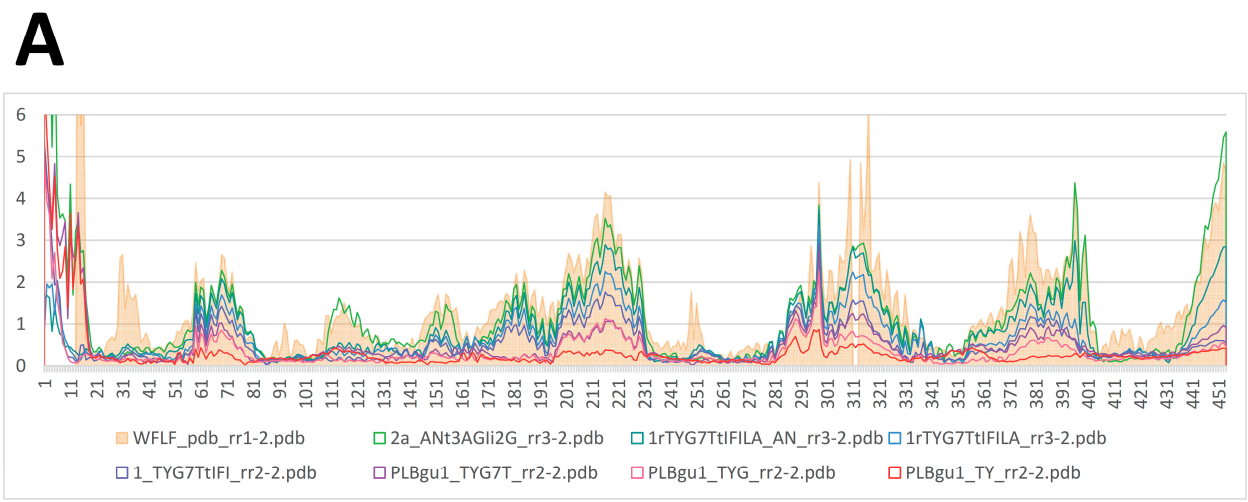

Figure 12. *Cont.*

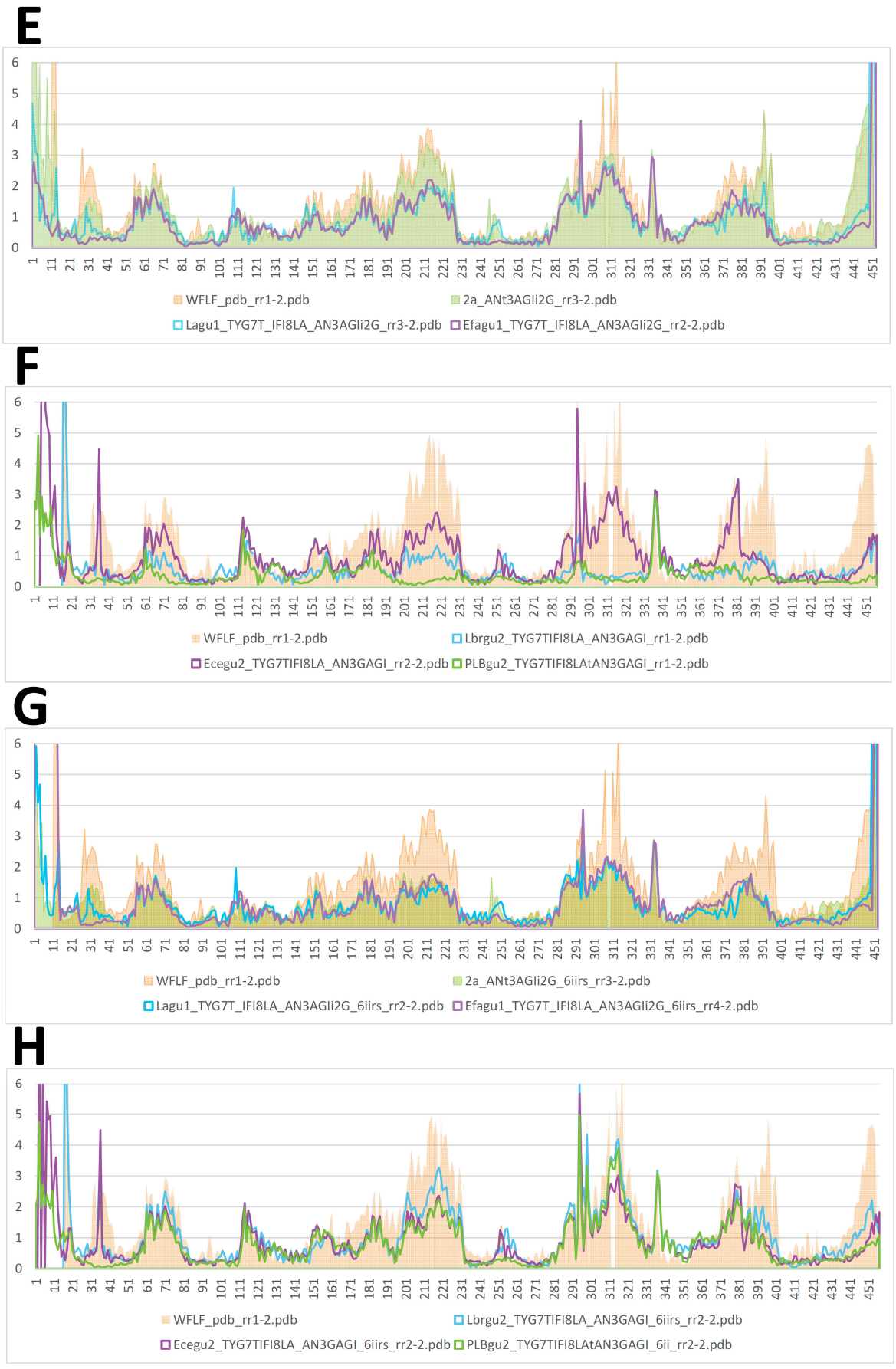

Figure 12. *Cont.*

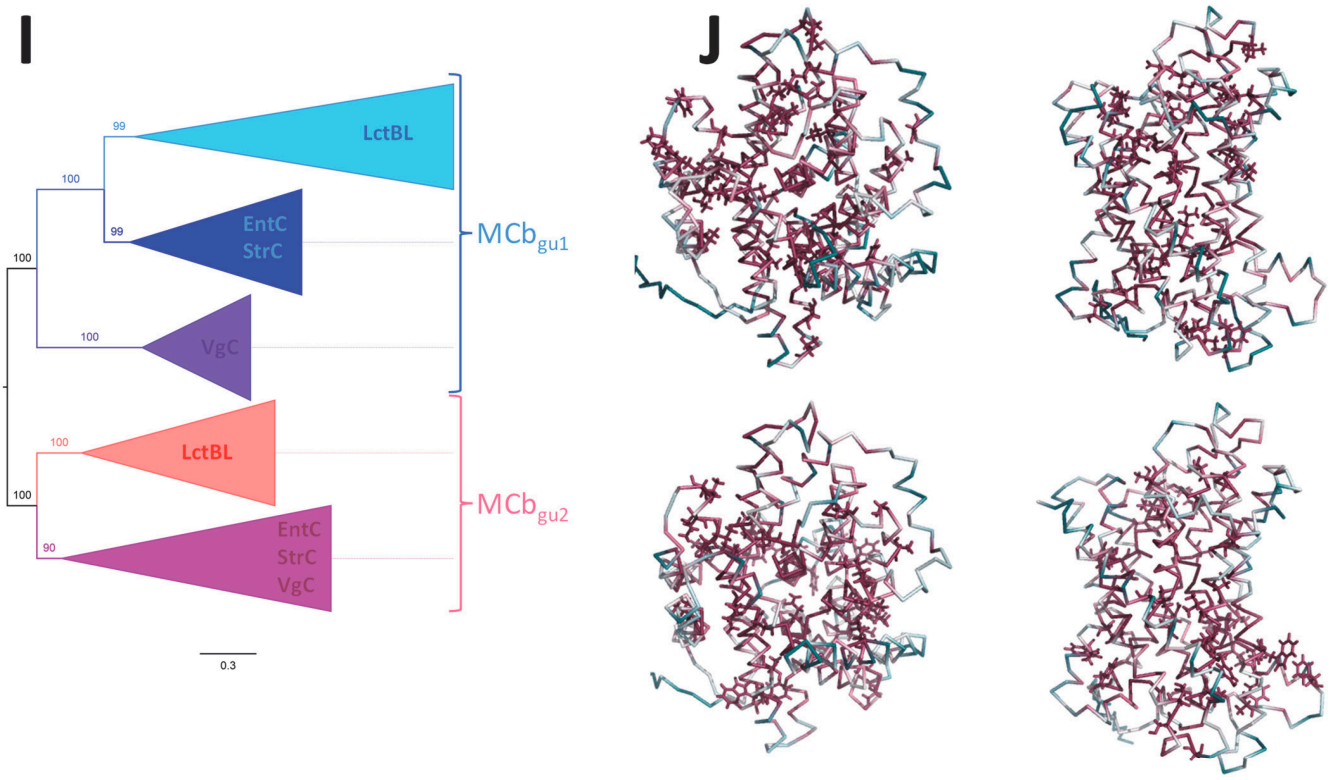

Figure 12. CFpdb modeling reveals functional differences between MCb$_{gu1}$ and MCb$_{gu2}$. (**A–C**) Mutagenesis-driven conformational change, from the outward open state toward inwardly open state, obtained by CFpdb modeling of compound PLB$_{gu1}$ mutants is shown as pRMSD from native PLB$_{gu1}$ model. The a.a. replacements targeted selectively conserved sites either across the Slc11 family (**B**) or among prototype Nramps (pN-I, pN-II) and MntH C clades (MCa, MCb, MCg and MCaU, [7]) (**C**). (**E**,**F**) Identical compound mutants LLB$_{gu1}$ (Lagu1) and EC$_{gu1}$ (Efagu1) display conformational responses like PLB$_{gu1,}$ while the mutants PLB$_{gu2}$, LLB$_{gu2}$ (Lbrgu2) and EC$_{gu2}$ (Ecegu2) exhibit more diverse overall shapes, shown as pRMSD from EC$_{gu1}$ (**E**) and PLB$_{gu2}$ (**F**) native 3D models. (**D**,**G**,**H**) Adding reciprocal mutations to exchange residues that distinguish MCb$_{gu1}$ from MCb$_{gu2}$ (**D**) impaired MCb$_{gu1}$ conformation similarly for all 3 templates (**G**), while some MCb$_{gu2}$ showed opposite effect (**H**), indicated by pRMSD from EC$_{gu1}$ (**G**) and PLB$_{gu2}$ (**H**) respective native 3D models (cf mutant Table S2). (**I**,**J**) Evolutionary divergence of MCb$_{gu1}$ and MCb$_{gu2}$ clades. Simplified IQ-Tree representation of MCb$_{gu1}$ and MCb$_{gu2}$ clade relationships ((**I**), 46 seqs each, detailed in Figure S7). Clade-specific Consurf evolutionary conservation patterns among MCb$_{gu1}$ (top, native EC$_{gu1}$ CF model, Efagu1) and MCb$_{gu2}$ (bottom, native EC$_{gu2}$ CF model, Ecegu2) clades (**J**). Model MCb carrier views of the outward face (left) and the transmembrane helix bundle (right).

3. Discussion

This in silico study correlates the emergence of LB with the functional divergence of a pair of (Slc11) MCb$_{gut}$ carriers. MCb$_{gut}$ carriers share a common ancestor with their sister clade MCb$_{ie}$, and together, they form the group MCb, which evolved from the group MCa. MCb$_{ie}$ predominates in marine Bacillaceae and demonstrates evolutionary conservation; it relates directly MCa to MCb$_{gut}$ because MCb$_{ie}$ seqs display non-overlapping patterns of identical residues with relatives from each group. Comparative studies between the sister clades MCb$_{ie}$ and MCb$_{gut}$ indicate functional innovation to open the inner gate of MCb$_{gut}$ carriers as well as MCb$_{gut}$-specific structural dynamics plasticity. Apparently, MCb$_{gut}$ could evolve from MCb$_{ie}$ in response to selective pressure that fosters functional divergence. Assuming this was the case, such evolutionary pressure indicated novel environmental conditions. It is hypothesized that the gastro-intestinal tract of early marine vertebrates

provided a novel niche conducive for the progressive evolution of an MCb_{ie}^{+} Bacillaceae into the ancestor of LB, which carried a pair of genes coding for distinct MCb_{gut}.

To what extent did the data gathered support the possibility that Mn-dependent, MCb_{gut}^{+} LB evolved from some Bacillaceae precursor adapted to marine environment? First, several bacterial orders enriched in MCa^{+} spp. (e.g., Cyanobacteria, Pseudomonadales (gamma proteobacteria, GPB), Burkholderiales (BPB), Rhodobacterales, Sphingomonadales, Hyphomicrobiales (Rhizobiales, APB)) [7] might have formed Precambrian subaerial microbial mats that could include *Bacillus* spp. [32,33]. Such a terrestrial setting would facilitate the acquisition of the *mntH* Cb_{ie} gene precursor (*mntH* Ca) by some *Bacillus* spp. Bacillaceae represent the primary source of the *mntH* Cb_{ie} gene, consistent with evidence of recent gene transfers toward different spp. of Paenibacillaceae (*Paenibacillus* and *Brevibacillus* spp.) in which *mntH* Ca dominates. And many MCb_{ie}^{+} genera are marine Bacillales found in deep-sea sediments (e.g., *Bacillus*, *Paenibacillus*, *Lysinibacillus* and *Terribacillus* spp.), while others populate various environments, including the gut of animals [34,35].

Second, while the MntH A (MA) type, which is ancestral to all *mntH* C genes that were derived from eukaryotic cells (Figure 1A, Table S1), predominates in Bacillaceae, a fraction of Bacillaceae spp. acquainted with marine environment adopted instead MCb_{ie}. MCb_{ie} phylogeny indicates genera such as *Lederbergia*, *Siminovitchia*, *Heyndrickxia*, and *Neobacillus* (Figure S1B, [36]) may have inherited *mntH* Cb_{ie} vertically. Their phylogeny suggests these species as more likely candidate precursors of LB than MA^{+} Bacillaceae, such as *B. subtilis* and *B. cereus*. Also, these marine Bacillaceae grow aerobically, which implies Fe-based metabolism, and some were recovered as well from a dairy environment or found in the gut of various animals. The emergence of MCb_{ie} from MCa in marine Bacillaceae could thus mark a first step in the adaptation to the gut of animals such as invertebrates.

A consolidated hypothesis may thus be viewed in successive steps (Figure 13) with (i) the emergence of MCa^{+} Bacillaceae within subaerial/terrestrial microbial mats, which also colonized marine habitat, (ii) the adaptation of marine MCb_{ie}^{+} Bacillaceae to the gut of invertebrates, and (iii) the selection of Mn-dependent LB carrying a pair of *mntH* Cb_{gut} genes in the gut of early vertebrates. Previous studies suggest an exchange of MA for MCa affected the coupling of the pmf to Mn^{2+} import [7], which could improve resistance to environmental stresses (e.g., dessication, temperature, osmotic stress) and provide a path toward adaption to an acidic environment through the evolution of MCa to MCb_{ie} and then to MCb_{gut}—a step shown to the impact opening of the inner gate to carry Mn^{2+} ions inside cells. Prior works on MCb_{gut} homologs revealed both the plasticity of their functional dynamics [6] and their efficient use by LB to pump Mn^{2+} in competitive environments [12].

Whether this LB evolution toward Mn-based metabolism matched the final design of the gastro-intestinal (GI) tract of early vertebrates is a matter of conjecture. But this possibility may provide an interesting angle to approach our intimate relationships with LB because vertebrate development owed to successive innovations following the differentiation of the pharynx at the entry of the digestive tract in chordates, including, for instance, the development of sensory organs and vertebrate novelties such as the spleen, individualized pancreas, heart innervation and the eye's own muscles [37,38], which might have fostered mutualistic interactions between emerging LB and their host.

Vertebrate inventions took place around the 1R whole genome duplication (WGD) that occurred in the early Cambrian and which produced, in particular, the archetype Nramp 'Ohnologs' Nramp1 and Dmt1 ([39–41] and Figure S8). *NRAMP1* (*SLC11A1*) expression depends on C/EBP [42,43] and dominates in the spleen, blood and tissue phagocytes, contributing to host resistance to infection [8,44]. Dmt1/Nramp2 (Slc11a2) catalyzes H^{+}-dependent Fe^{2+} import both as part of the transferrin endocytic cycle that delivers iron through the body and at the apical membrane of duodenal enterocytes [45,46]. This context may suggest the Ediacaran transition to early Cambrian as a possible evolutionary interval for LB emergence while the GI tractus of early vertebrates was developing into its final form.

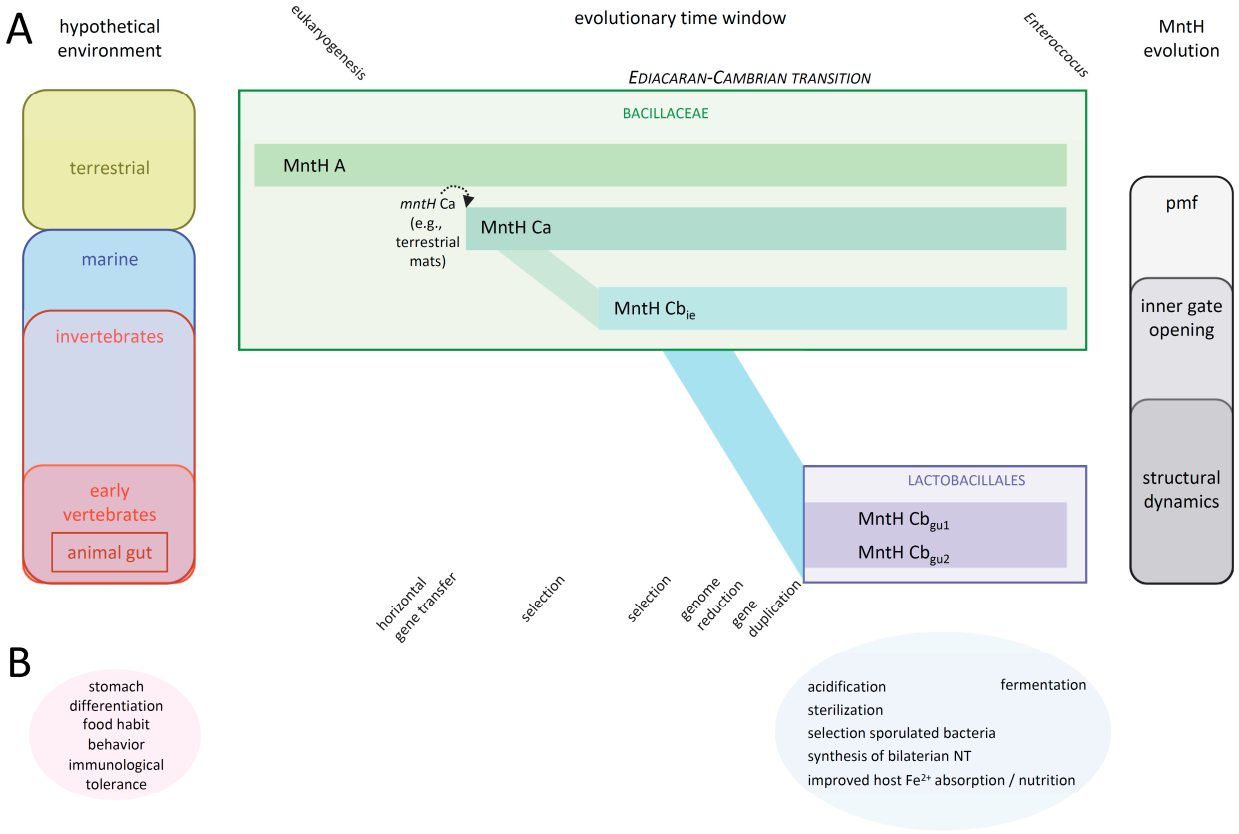

Figure 13. Hypothetical emergence of LB in the gut of early vertebrates based on molecular genetic and structural evolutionary analyses of Slc11 clade MCb (MCb_{ie} and MCb_{gut}, i.e., MCb_{gu1} and MCb_{gu2}). (**A**) The evolutionary time window considered is indicated to be from eukaryogenesis, ca. 2 billion years ago, to emergence of the genus *Enterococcus*, ca. 425 million years ago. It is proposed LB evolved during the Ediacaran–Cambrian transition (635–485 mya), possibly in the early Cambrian (ca. 540 mya). Substitution of the ancestral *mntH* A gene for a horizontally acquired *mntH* Ca gene is posited as initial step (MntH Ca^{+} Bacillaceae), followed by a combination of selective processes, including genome reduction and gene duplication. Successive environmental changes that could favor evolution of MCb (left) and previously reported stepwise changes in MntH functional properties (right) are indicated (from top to bottom). (**B**) LB colonization of the gut of protochordates led to acidification of the upper part of the gut during food fermentation, producing outcomes that could foster the establishment of the vertebrate gastro-intestinal tract in its canonical form (right panel), by emulating developmental host functions such as differentiation of the stomachal pouch, food habits and behavioral responses, and immunological tolerance (left panel).

High efficiency Mn intracellular accumulation under acidic conditions makes physiological sense for LB because Mn as a micronutrient accelerates their growth under lactate stress [47]. The lactic acidification of an LB environment has important effects on the GI tract: inhibiting the growth of potential microbial pathogens while providing a nutrient for potentially beneficial bacteria, such as the spore-forming component of the colonic microbiota [48], which, by consuming lactate that is transformed into short-chain fatty acids (SCFAs), may stimulate LB growth in return [49,50]. These effects, added to LB's ability to predigest complex foods could possibly help develop the GI tract of early vertebrates by favoring the differentiation of the gastric organ (stomach).

The GI tracts of urochordates and cephalochordates comprise organs homologous to the liver and pancreas of vertebrates, and chordates share the molecular basis of extracellular digestion with vertebrates. Yet, their genomes lack the *pepsinogen* gene encoding a gastric digestive enzyme and cephalochordates demonstrate evidence of intracellular digestion in the hepatic cecum. This suggests that extracellular digestion systems based

on both stomach and pancreatic digestive enzymes emerged specifically in the common ancestor of vertebrates ([51,52] and based on the homologs of GTEx stomach-specific encoded polypeptides, [53], detected in Cephalochordates: Lipase F, gastric type >50% aa id; in Chondrichthyes: Pepsinogen >60% aa id; in Tetrapods: Trefoil factor 1 & 2, >67% aa id).

LB strains isolated from mammalian source (mainly rodents) colonize the gastric epithelium by forming biofilms [18,54–56]. To resist the harsh environment of the stomach lumen, LB use glutamate and aromatic L-amino acid decarboxylases which help in sustaining the transmembrane pmf to energize metabolism and transport [57,58]. The fact that these bacterial enzymes produce amino acid-derived compounds used as neurotransmitters (NTs) in bilaterian animals [59], such as serotonine, dopamine and GABA [55], both in the central nervous system (CNS) and the enteric nervous system (ENS) [60], suggests a possible feed forward loop [61] where proto-LB residing in the upper gut of some vertebrate ancestor would respond to food intake by generating an acidic environment, facilitating digestion and contributing to gut–brain signaling.

An acidic environment in the duodenum of vertebrates is key for absorbing the growth supporting micronutrient iron in the form of Fe^{2+} [46]. As it seems, selection of duodenal Slc11a2- and H^+-dependent Fe^{2+} uptake may thus correspond to the period of the establishment of the vertebrate stomach. And the prospect that these processes were supported by Mn^{2+}-dependent acid-resistant LB expressing MCb_{gut} parologs may bear significance in terms of distinct substrate selectivity among Slc11 homologs and the partition of micronutrient resources for mutual benefits [62] to the vertebrate host (Fe) and to the LB residing in its gut (Mn). Arguably, an example of ecological–evolutionary interaction [61,63,64] that provided a rich foundation to diversify vertebrate holobionts.

Previous in silico data obtained with MCb_{gut} demonstrated highly plastic structural dynamics that may increase Mn import efficiency, hereby sustaining LB resistance to acidic and osmotic stress. Herein, a further study of MCb_{gut} revealed a parology that predated LB radiation, while the sister carrier MCb_{ie} showed structural differences likely altering Mn intracellular release. These data may suggest that the evolution of LB MCb_{gut} could foster a novel, Mn-dependent way of life in an acidic environment stocked up with food while relinquishing the use of Fe to their host. This process was likely progressive, contracting LB's ancestral $MCb_{ie}{}^+$ Bacillaceae genome and going along with the differentiation of the stomachal pouch as a specialized organ in the neo gastro-intestinal tract of the ancestor of jawed vertebrates.

Gastric LB could impact host behavior and food habits through the synthesis of NTs that act directly on leukocytes within the GI tract lamina propria and affect nerve ganglia of the ENS, producing signals relayed through afferent vagal connections to the CNS [65,66]. These instructions could be modulated by intestinal SCFA-producing bacteria, which may act directly on vagal intestinal terminals and stimulate NT signals [67]. In return, efferent vagal influx from the CNS toward the spleen produces NTs that directly regulate the secretion of proinflammatory cytokines by leukocytes [68]. Similarly, enteric bacteria could also modulate local steroid secretion, contributing to reduce stress hormone levels and inform the CNS to adjust behavioral output [60]. It would seem possible that the emergence of LB is owed at least partly to their ability to communicate with their host via the gut–brain axis.

Vertebrate transition to extracellular intestinal digestion presented inherent risks that required immunological surveillance because luminal microbes opting for a pathogenic lifestyle may weaken the intestinal barrier's integrity and create a portal for host infection [69,70]. Viewing regulatory lymphocytes as metabolic sensors, the fact that Tregs mediate suppressive functions when food is scarce, whereas the inflammatory functions of Th17 are fueled by glycolysis [71,72], suggests food digestion potentially incurs intestinal inflammation that depends on subsequent resolution to maintain homeostasis and develop immune tolerance to food-derived determinants [73]. Also, lactic acid sensing has an anti-inflammatory effect by modulating macrophage phenotype polarization [74,75]. According to these views, gut LB and SCFA producers and their metabolites could directly instruct

the emerging adaptive immune system while sustaining systemic innate immunity due to Firmicutes intrinsic lysozyme sensitivity [76].

Also, both lymphocyte and erythrocyte cell types emerged as vertebrate specificities [77]. Duodenal Fe absorption boosted with gastric acidification likely helped develop the erythron (e.g., hetero-tetrameric hemoglobin in jawed vertebrates, [78]) to distribute oxygen within tissues and sustain their metabolic activity. Apparently, LB Mn-based metabolism and gastric acidification could thus enhance host Fe- and oxygen-based metabolism. And combined with their behavioral and immunological influence, LB's role in stimulating host metabolism could elevate energetic efficiency and help diversify early vertebrates. The divergence of LB families may have been contemporaneous, perhaps reflecting various mutualist interactions implemented by diverse hosts.

According to recent views, the Ediacaran–Cambrian transition, which produced animal radiation, could be due to a combination of causes, including transient catastrophic events (snowball earths and hypoxic environments) and progressive 'biotic replacement' through successive pulses of evolutionary innovations and ecosystem engineering [79–84]. The 1R genome duplication that occurred prior to the divergence of jawed vertebrates may indeed testify to disruptive environmental changes during this period. On the other hand, the ability of extant LB probiotics to regulate mammalian brain, digestive and immune activity [55,60,66] suggests that emerging Mn-dependent MCb_{gut}^{+} LB colonizers, adapted to the upper gut of ancestral vertebrates, could impact the feeding habits and behavior of their host, thereby influencing its evolution [85,86].

Hence, a LB-driven feed forward loop may have contributed to diversify early vertebrate body plans, and turning to jawless vertebrates may be instructive in this regard. The sea lamprey has a life cycle comprising three distinct stages: blind larvae burrowing into the sand feeding on microbes and detritus by filtering surrounding water; the first metamorphosis rearranges sensory organs, forms a new esophagus and modifies the digestive system of free living juvenile lampreys that display high diet conversion efficiency and temperature-dependent growth; the second metamorphosis atrophies the intestine of fasting adults that die after spawning [87,88]. Apparently, the microbiota associated with growing wild juveniles is selectively enriched in LB, *Streptococcus* spp., in particular. Regarding hagfish gut microbiota, a close relative of LB *Weissella cibaria* (MCb_{gut}^{+}) was detected in wild *Eptatretus,* while in captive specimens, MntH A^{+} enterobacteria dominate (Figure S9). These data support the notion that gut LB could directly contribute to the growth and development of early vertebrates. However, continuous host development, perhaps tributary of further innovations such as jaws, heterodimeric hemoglobin and myelinization as well as the 2R genome allotetraploidization [39,40,78,89], was likely required to further vertebrate radiation and inflate marine biodiversity by fueling an evolutionary arms race toward ever more efficient predators [81,90].

In sum, it is proposed that MCb_{gut}^{+} LB emerged in the upper gut of early vertebrates (ca. 540 mya, i.e., prior to vertebrate 1R WGD). LB colonization formed a novel holobiont that prefigured the final design of the gastro-intestinal tract of jawed vertebrates, whose development could benefit from boosted nutritional efficiency procured through LB–host interactions. Establishing a feed forward loop for food access and tolerance could incentivize LB genome reduction and adaptation as Mn-dependent gastric aids, while their pro-gastric functions stimulated vertebrate Fe-dependent growth and development. Accordingly, LB evolution involved successive phases: (i) reductive, during marine MCb_{ie}^{+} Bacillaceae adaptation to early vertebrate upper gut, leading to Mn-centric, acid-resistant fermentative cells (MCb_{gut}^{+} LB); and (ii) expansive, through the subsequent dissemination of MCb_{gut}^{+} LB adapting to novel niches, including terrestrial environments. Molecular communication between extant LB and the mammalian gut–brain axis and immune system may include remnants of early vertebrate pro-gastric functions and subsequent interactions between more evolved organisms.

4. Materials and Methods

Protein sequences were collected using NCBI and Uniprot repositories and BLAST programs (PHI-BLAST, TBLASTN and BLASTP, [91]). Sequences were curated using the MPI toolkit and the MMseqs2 program to retrieve sets of diverse seqs with reduced complexity [92]. ClustalX [93] seqs clustering and graphic display was used to unambiguously classify seqs into established phylogroups, using reference seqs [7].

Each phylogenetic analysis was performed using a balanced set of groups of seqs to be analyzed plus a defined outgroup. Multiple seqs were aligned using Muscle [94] and the resulting alignments were manually edited using Seaview [95]. As needed, a Phylo-mLogo [96] display of the multiple sequence alignment was generated by writing a simple tree, aggregating clade-specific sets of seqs. Multiple sequence alignments were trimmed to eliminate sites with gaps or judged poorly informative in the Phylo-mLogo display, using Treecon [97]. Parsimony-informative sites were selected using Mega [98]. Tree calculations with IQ-Tree [99] used a number of categories of the free-rate heterogeneity model that was commensurate with the length of the parsimony-informative site alignment to estimate variations in substitution rate among sites using proportions of site categories and mixture substitution matrices [100]. Trees were displayed using FigTree (Version—v1.4.4; http://tree.bio.ed.ac.uk/software/figtree/ (accessed on 1 August 2024)) to appreciate the statistical robustness of tree nodes.

Site selection for mutagenesis used defined phylogroups of aligned seqs to identify candidate type ii evolutionary rate-shifts, distinguishing the groups under study [4] based on the Sequence Harmony and Multi-Relief approaches [101]. Sites producing highly significant scores with both approaches were selected as sets of coevolved sites discriminating sister phylogroups. Reciprocal mutagenesis was performed by exchanging sets of phylogroup-specific residues between templates from each group. Additional mutations targeted sites defining the family of Slc11 carriers (Slc11 synapomorphy) as well as sites that characterize clades part of the Slc11 family. Every point mutation introduced was verified a posteriori with the returned seq of the predicted model. Differences in evolutionary rates between sister clades were also visualized using Consurf [102].

3D modeling was performed using CF [11] with or without template (CFpdb and CFnt, respectively) and native seqs to identify the training model producing the best model, which was used to analyze corresponding mutant seqs [6]. AF2 models were retrieved from the Uniprot repository [103]. Molecular analyses using 2StrucCompare [104] allowed us to determine per residue the root mean square deviation of the Ca trace between pairs of aligned structures, which was visualized using spreadsheet software. The All Against All program (Dali EBI, [105]) was used to establish the 3D correspondence of groups of structures based on pairwise comparisons. POSA [106] was used to obtain multiple flexibly superimposed structures. Structures were visualized using Pymol (DeLano, W.L. The PyMOL Molecular Graphics System; Delano Scientific: San Carlos, CA, USA, 2002).

Supplementary Materials: The following supporting information can be downloaded at https://www.mdpi.com/article/10.3390/bacteria3030016/s1, Figure S1: MCb (MCb_{ie} and MCb_{gut}) phylogeny among bacterial families comprising MCb_{ie}^{+} spp.; Figure S2: Phylogenomic analyses of select LB, Bacillaceae, Listeriaceae and Staphylococcaceae spp.; Figure S3: Phylo-mLogo display of site-specific sequence variations in extra-membranous loops between aligned seqs from the MntH C groups MCa, MCb_{ie} and MCb_{gut}; Figure S4: CFnt modeling of *Terribacillus aidingensis* MCb_{ie} A0A285P4W2 responds to mutagenesis like A0A143Y4E1 from *Trichochoccus palustris*; Figure S5: MCb_{gut} phylogeny in the Enterococcaceae family; Figure S6: CFpdb modeling shows MCb_{gu1} and MCb_{gu2} structural dynamics differ; Figure S7: MCb_{gu1} and MCb_{gu2} unrooted phylogeny; Figure S8: Divergence of archetype Nramp parologs Nramp1 and Dmt1 followed the 1R whole genome that took place in early vertebrates; Figure S9: The gut microbiota of wild hagfishes may be enriched in MCb_{gut}^{+} bacteria; Table S1: Slc11 carrier nomenclature, taxonomic distribution (representative taxa) and origin; Table S2: Mutants produced in this study.

Funding: This research received no external funding.

Data Availability Statement: The models and sequences used in this study are included in Non-published Material.

Acknowledgments: The providers and caretakers of the online services, servers and repositories that were used for this work are gratefully acknowledged. I thank Stella Cellier-Goetghebeur for her comments and suggestions to improve this manuscript.

Conflicts of Interest: The author declares no conflicts of interest.

References

1. Del Alamo, D.; Meiler, J.; McHaourab, H.S. Principles of Alternating Access in LeuT-fold Transporters: Commonalities and Divergences. *J. Mol. Biol.* **2022**, *434*, 167746. [CrossRef] [PubMed]
2. Manatschal, C.; Dutzler, R. The Structural Basis for Metal Ion Transport in the SLC11/NRAMP Family. *Chimia* **2022**, *76*, 1005–1010. [CrossRef] [PubMed]
3. Ray, S.; Gaudet, R. Structures and coordination chemistry of transporters involved in manganese and iron homeostasis. *Biochem. Soc. Trans.* **2023**, *51*, 897–923. [CrossRef] [PubMed]
4. Cellier, M.F. Nramp: From sequence to structure and mechanism of divalent metal import. *Curr. Top. Membr.* **2012**, *69*, 249–293. [PubMed]
5. Marinelli, F.; Faraldo-Gomez, J.D. Conformational free-energy landscapes of a Na^+/Ca^{2+} exchanger explain its alternating-access mechanism and functional specificity. *Proc. Natl. Acad. Sci. USA* **2024**, *121*, e2318009121. [CrossRef] [PubMed]
6. Cellier, M.F.M. Slc11 Synapomorphy: A Conserved 3D Framework Articulating Carrier Conformation Switch. *Int. J. Mol. Sci.* **2023**, *24*, 15076. [CrossRef]
7. Cellier, M.F.M. Nramp: Deprive and conquer? *Front. Cell Dev. Biol.* **2022**, *10*, 988866. [CrossRef]
8. Casanova, J.L.; MacMicking, J.D.; Nathan, C.F. Interferon-gamma and infectious diseases: Lessons and prospects. *Science* **2024**, *384*, eadl2016. [CrossRef]
9. Cellier, M.F.; Bergevin, I.; Boyer, E.; Richer, E. Polyphyletic origins of bacterial Nramp transporters. *Trends. Genet.* **2001**, *17*, 365–370. [CrossRef]
10. Jumper, J.; Evans, R.; Pritzel, A.; Green, T.; Figurnov, M.; Ronneberger, O.; Tunyasuvunakool, K.; Bates, R.; Zidek, A.; Potapenko, A.; et al. Highly accurate protein structure prediction with AlphaFold. *Nature* **2021**, *596*, 583–589. [CrossRef]
11. Mirdita, M.; Schütze, K.; Moriwaki, Y.; Heo, L.; Ovchinnikov, S.; Steinegger, M. ColabFold: Making protein folding accessible to all. *Nat. Methods* **2022**, *19*, 679–682. [CrossRef] [PubMed]
12. Bosma, E.F.; Rau, M.H.; van Gijtenbeek, L.A.; Siedler, S. Regulation and distinct physiological roles of manganese in bacteria. *FEMS Microbiol. Rev.* **2021**, *45*, fuab028. [CrossRef] [PubMed]
13. Karlsen, S.T.; Rau, M.H.; Sanchez, B.J.; Jensen, K.; Zeidan, A.A. From genotype to phenotype: Computational approaches for inferring microbial traits relevant to the food industry. *FEMS Microbiol. Rev.* **2023**, *47*, fuab028, fuad030. [CrossRef] [PubMed]
14. Makarova, K.; Slesarev, A.; Wolf, Y.; Sorokin, A.; Mirkin, B.; Koonin, E.; Pavlov, A.; Pavlova, N.; Karamychev, V.; Polouchine, N.; et al. Comparative genomics of the lactic acid bacteria. *Proc. Natl. Acad. Sci. USA* **2006**, *103*, 15611–15616. [CrossRef]
15. Makarova, K.S.; Koonin, E.V. Evolutionary genomics of lactic acid bacteria. *J. Bacteriol.* **2007**, *189*, 1199–1208. [CrossRef] [PubMed]
16. Huynh, U.; Qiao, M.; King, J.; Trinh, B.; Valdez, J.; Haq, M.; Zastrow, M.L. Differential Effects of Transition Metals on Growth and Metal Uptake for Two Distinct Lactobacillus Species. *Microbiol. Spectr.* **2022**, *10*, e0100621. [CrossRef] [PubMed]
17. Elli, M.; Zink, R.; Rytz, A.; Reniero, R.; Morelli, L. Iron requirement of Lactobacillus spp. in completely chemically defined growth media. *J. Appl. Microbiol.* **2000**, *88*, 695–703. [CrossRef] [PubMed]
18. Li, F.; Li, X.; Cheng, C.C.; Bujdos, D.; Tollenaar, S.; Simpson, D.J.; Tasseva, G.; Perez-Munoz, M.E.; Frese, S.; Ganzle, M.G.; et al. phylogenomic analysis of Limosilactobacillus reuteri reveals ancient and stable evolutionary relationships with rodents and birds and zoonotic transmission to humans. *BMC Biol.* **2023**, *21*, 53. [CrossRef] [PubMed]
19. Koga, Y. Microbiota in the stomach and application of probiotics to gastroduodenal diseases. *World J. Gastroenterol.* **2022**, *28*, 6702–6715. [CrossRef]
20. Lebreton, F.; Manson, A.L.; Saavedra, J.T.; Straub, T.J.; Earl, A.M.; Gilmore, M.S. Tracing the Enterococci from Paleozoic Origins to the Hospital. *Cell* **2017**, *169*, 849–861.e13. [CrossRef]
21. Weller, D.; Andrus, A.; Wiedmann, M.; den Bakker, H.C. Listeria booriae sp. nov. and Listeria newyorkensis sp. nov., from food processing environments in the USA. *Int. J. Syst. Evol. Microbiol.* **2015**, *65 Pt 1*, 286–292. [CrossRef] [PubMed]
22. Maayer, P.; Aliyu, H.; Cowan, D.A. Reorganising the order Bacillales through phylogenomics. *Syst. Appl. Microbiol.* **2019**, *42*, 178–189. [CrossRef] [PubMed]
23. Collins, M.D.; Wallbanks, S.; Lane, D.J.; Shah, J.; Nietupski, R.; Smida, J.; Dorsch, M.; Stackebrandt, E. Phylogenetic analysis of the genus Listeria based on reverse transcriptase sequencing of 16S rRNA. *Int. J. Syst. Bacteriol.* **1991**, *41*, 240–246. [CrossRef]
24. Tian, R.; Imanian, B. VBCG: 20 validated bacterial core genes for phylogenomic analysis with high fidelity and resolution. *Microbiome* **2023**, *11*, 247. [CrossRef] [PubMed]
25. Sun, J.; Lu, F.; Luo, Y.; Bie, L.; Xu, L.; Wang, Y. OrthoVenn3: An integrated platform for exploring and visualizing orthologous data across genomes. *Nucleic Acids Res.* **2023**, *51*, W397–W403. [CrossRef]

26. van Dijk, M.C.; de Kruijff, R.M.; Hagedoorn, P.L. The Role of Iron in Staphylococcus aureus Infection and Human Disease: A Metal Tug of War at the Host-Microbe Interface. *Front. Cell Dev. Biol.* **2022**, *10*, 857237. [CrossRef]
27. McLaughlin, H.P.; Hill, C.; Gahan, C.G. The impact of iron on Listeria monocytogenes; inside and outside the host. *Curr. Opin. Biotechnol.* **2011**, *22*, 194–199. [CrossRef] [PubMed]
28. Ehrnstorfer, I.A.; Manatschal, C.; Arnold, F.M.; Laederach, J.; Dutzler, R. Structural and mechanistic basis of proton-coupled metal ion transport in the SLC11/NRAMP family. *Nat. Commun.* **2017**, *8*, 14033. [CrossRef]
29. Ehrnstorfer, I.A.; Geertsma, E.R.; Pardon, E.; Steyaert, J.; Dutzler, R. Crystal structure of a SLC11 (NRAMP) transporter reveals the basis for transition-metal ion transport. *Nat. Struct. Mol. Biol.* **2014**, *21*, 990–996. [CrossRef]
30. Schwartzman, J.A.; Lebreton, F.; Salamzade, R.; Shea, T.; Martin, M.J.; Schaufler, K.; Urhan, A.; Abeel, T.; Camargo, I.; Sgardioli, B.F.; et al. Global diversity of enterococci and description of 18 previously unknown species. *Proc. Natl. Acad. Sci. USA* **2024**, *121*, e2310852121. [CrossRef]
31. Richer, E.; Courville, P.; Bergevin, I.; Cellier, M.F. Horizontal gene transfer of "prototype" Nramp in bacteria. *J. Mol. Evol.* **2003**, *57*, 363–376. [CrossRef] [PubMed]
32. Finke, N.; Simister, R.L.; O'Neil, A.H.; Nomosatryo, S.; Henny, C.; MacLean, L.C.; Canfield, D.E.; Konhauser, K.; Lalonde, S.V.; Fowle, D.A.; et al. Mesophilic microorganisms build terrestrial mats analogous to Precambrian microbial jungles. *Nat. Commun.* **2019**, *10*, 4323. [CrossRef]
33. Lenton, T.M.; Daines, S.J. Matworld—The biogeochemical effects of early life on land. *New Phytol.* **2017**, *215*, 531–537. [CrossRef] [PubMed]
34. Ettoumi, B.; Guesmi, A.; Brusetti, L.; Borin, S.; Najjari, A.; Boudabous, A.; Cherif, A. Microdiversity of deep-sea Bacillales isolated from Tyrrhenian sea sediments as revealed by ARISA, 16S rRNA gene sequencing and BOX-PCR fingerprinting. *Microbes Environ.* **2013**, *28*, 361–369. [CrossRef] [PubMed]
35. Mandic-Mulec, I.; Stefanic, P.; van Elsas, J.D. Ecology of Bacillaceae. *Microbiol. Spectr.* **2015**, *3*, TBS-0017-2013. [CrossRef]
36. Gupta, R.S.; Patel, S.; Saini, N.; Chen, S. Robust demarcation of 17 distinct *Bacillus* species clades, proposed as novel Bacillaceae genera, by phylogenomics and comparative genomic analyses: Description of *Robertmurraya kyonggiensis* sp. nov. and proposal for an emended genus *Bacillus* limiting it only to the members of the Subtilis and Cereus clades of species. *Int. J. Syst. Evol. Microbiol.* **2020**, *70*, 5753–5798, Erratum in *Int. J. Syst. Evol. Microbiol.* **2020**, *70*, 6531–6533.
37. Shimeld, S.M.; Holland, P.W. Vertebrate innovations. *Proc. Natl. Acad. Sci. USA* **2000**, *97*, 4449–4452. [CrossRef] [PubMed]
38. Grillner, S. Evolution of the vertebrate motor system—From forebrain to spinal cord. *Curr. Opin. Neurobiol.* **2021**, *71*, 11–18. [CrossRef] [PubMed]
39. Yu, D.; Ren, Y.; Uesaka, M.; Beavan, A.J.S.; Muffato, M.; Shen, J.; Li, Y.; Sato, I.; Wan, W.; Clark, J.W.; et al. Hagfish genome elucidates vertebrate whole-genome duplication events and their evolutionary consequences. *Nat. Ecol. Evol.* **2024**, *8*, 519–535. [CrossRef] [PubMed]
40. Marletaz, F.; Timoshevskaya, N.; Timoshevskiy, V.A.; Parey, E.; Simakov, O.; Gavriouchkina, D.; Suzuki, M.; Kubokawa, K.; Brenner, S.; Smith, J.J.; et al. The hagfish genome and the evolution of vertebrates. *Nature* **2024**, *627*, 811–820. [CrossRef]
41. Sassa, M.; Takagi, T.; Kinjo, A.; Yoshioka, Y.; Zayasu, Y.; Shinzato, C.; Kanda, S.; Murakami-Sugihara, N.; Shirai, K.; Inoue, K. Divalent metal transporter-related protein restricts animals to marine habitats. *Commun. Biol.* **2021**, *4*, 463. [CrossRef]
42. Richer, E.; Campion, C.G.; Dabbas, B.; White, J.H.; Cellier, M.F. Transcription factors Sp1 and C/EBP regulate NRAMP1 gene expression. *FEBS J.* **2008**, *275*, 5074–5089. [CrossRef] [PubMed]
43. Cellier, M.F.M. Developmental Control of NRAMP1 (SLC11A1) Expression in Professional Phagocytes. *Biology* **2017**, *6*, 28. [CrossRef] [PubMed]
44. Raberg, L. Human and pathogen genotype-by-genotype interactions in the light of coevolution theory. *PLoS Genet.* **2023**, *19*, e1010685. [CrossRef]
45. Galy, B.; Conrad, M.; Muckenthaler, M. Mechanisms controlling cellular and systemic iron homeostasis. *Nat. Rev. Mol. Cell Biol.* **2024**, *25*, 133–155. [CrossRef]
46. Shawki, A.; Anthony, S.R.; Nose, Y.; Engevik, M.A.; Niespodzany, E.J.; Barrientos, T.; Ohrvik, H.; Worrell, R.T.; Thiele, D.J.; Mackenzie, B. Intestinal DMT1 is critical for iron absorption in the mouse but is not required for the absorption of copper or manganese. *Am. J. Physiol. Gastrointest. Liver. Physiol.* **2015**, *309*, G635–G647. [CrossRef]
47. Zhang, K.; Zhang, Z.; Guo, X.; Guo, R.; Zhu, L.; Qiu, X.; Yu, X.; Chai, J.; Gu, C.; Feng, Z. Changes in nutrient consumption patterns of Lactobacillus fermentum mediated by sodium lactate. *J. Sci. Food Agric.* **2023**, *103*, 1775–1783. [CrossRef]
48. de Hoon, M.J.; Eichenberger, P.; Vitkup, D. Hierarchical evolution of the bacterial sporulation network. *Curr. Biol.* **2010**, *20*, R735–R745. [CrossRef]
49. Morrison, D.J.; Preston, T. Formation of short chain fatty acids by the gut microbiota and their impact on human metabolism. *Gut Microbes* **2016**, *7*, 189–200. [CrossRef] [PubMed]
50. Sereti, I.; Verburgh, M.L.; Gifford, J.; Lo, A.; Boyd, A.; Verheij, E.; Verhoeven, A.; Wit, F.; Schim van der Loeff, M.F.; Giera, M.; et al. Impaired gut microbiota-mediated short-chain fatty acid production precedes morbidity and mortality in people with HIV. *Cell Rep.* **2023**, *42*, 113336. [CrossRef]
51. Nakayama, S.; Sekiguchi, T.; Ogasawara, M. Molecular and evolutionary aspects of the protochordate digestive system. *Cell Tissue Res.* **2019**, *377*, 309–320. [CrossRef]

52. Castro, L.F.; Goncalves, O.; Mazan, S.; Tay, B.H.; Venkatesh, B.; Wilson, J.M. Recurrent gene loss correlates with the evolution of stomach phenotypes in gnathostome history. *Proc. Biol. Sci.* **2014**, *281*, 20132669. [CrossRef] [PubMed]
53. Consortium, G.T. The Genotype-Tissue Expression (GTEx) project. *Nat. Genet.* **2013**, *45*, 580–585.
54. Suzuki-Hashido, N.; Tsuchida, S.; Hayakawa, T.; Sakamoto, M.; Azumano, A.; Seino, S.; Matsuda, I.; Ohkuma, M.; Ushida, K. Lactobacillus nasalidis sp. nov., isolated from the forestomach of a captive proboscis monkey (Nasalis larvatus). *Int. J. Syst. Evol. Microbiol.* **2021**, *71*, 004787. [CrossRef] [PubMed]
55. Yuan, C.; He, Y.; Xie, K.; Feng, L.; Gao, S.; Cai, L. Review of microbiota gut brain axis and innate immunity in inflammatory and infective diseases. *Front. Cell. Infect. Microbiol.* **2023**, *13*, 1282431. [CrossRef] [PubMed]
56. Duar, R.M.; Lin, X.B.; Zheng, J.; Martino, M.E.; Grenier, T.; Perez-Munoz, M.E.; Leulier, F.; Ganzle, M.; Walter, J. Lifestyles in transition: Evolution and natural history of the genus Lactobacillus. *FEMS Microbiol. Rev.* **2017**, *41* (Suppl. S1), S27–S48. [CrossRef] [PubMed]
57. Perez, M.; Calles-Enriquez, M.; Nes, I.; Martin, M.C.; Fernandez, M.; Ladero, V.; Alvarez, M.A. Tyramine biosynthesis is transcriptionally induced at low pH and improves the fitness of Enterococcus faecalis in acidic environments. *Appl. Microbiol. Biotechnol.* **2015**, *99*, 3547–3558. [CrossRef] [PubMed]
58. Pereira, C.I.; Matos, D.; San Romao, M.V.; Crespo, M.T. Dual role for the tyrosine decarboxylation pathway in Enterococcus faecium E17: Response to an acid challenge and generation of a proton motive force. *Appl. Environ. Microbiol.* **2009**, *75*, 345–352. [CrossRef]
59. Goulty, M.; Botton-Amiot, G.; Rosato, E.; Sprecher, S.G.; Feuda, R. The monoaminergic system is a bilaterian innovation. *Nat. Commun.* **2023**, *14*, 3284. [CrossRef]
60. Cryan, J.F.; O'Riordan, K.J.; Cowan, C.S.M.; Sandhu, K.V.; Bastiaanssen, T.F.S.; Boehme, M.; Codagnone, M.G.; Cussotto, S.; Fulling, C.; Golubeva, A.V.; et al. The Microbiota-Gut-Brain Axis. *Physiol. Rev.* **2019**, *99*, 1877–2013. [CrossRef]
61. Decaestecker, E.; Van de Moortel, B.; Mukherjee, S.; Gurung, A.; Stoks, R.; De Meester, L. Hierarchical eco-evo dynamics mediated by the gut microbiome. *Trends Ecol. Evol.* **2024**, *39*, 165–174. [CrossRef]
62. Tannock, G.W.; Wilson, C.M.; Loach, D.; Cook, G.M.; Eason, J.; O'Toole, P.W.; Holtrop, G.; Lawley, B. Resource partitioning in relation to cohabitation of Lactobacillus species in the mouse forestomach. *ISME J.* **2012**, *6*, 927–938. [CrossRef] [PubMed]
63. Shankregowda, A.M.; Siriyappagouder, P.; Kuizenga, M.; Bal, T.M.P.; Abdelhafiz, Y.; Eizaguirre, C.; Fernandes, J.M.O.; Kiron, V.; Raeymaekers, J.A.M. Host habitat rather than evolutionary history explains gut microbiome diversity in sympatric stickleback species. *Front. Microbiol.* **2023**, *14*, 1232358. [CrossRef] [PubMed]
64. Baldo, L.; Pretus, J.L.; Riera, J.L.; Musilova, Z.; Bitja Nyom, A.R.; Salzburger, W. Convergence of gut microbiotas in the adaptive radiations of African cichlid fishes. *ISME J.* **2017**, *11*, 1975–1987. [CrossRef]
65. Gaskill, P.J.; Khoshbouei, H. Dopamine and norepinephrine are embracing their immune side and so should we. *Curr. Opin. Neurobiol.* **2022**, *77*, 102626. [CrossRef] [PubMed]
66. Decarie-Spain, L.; Hayes, A.M.R.; Lauer, L.T.; Kanoski, S.E. The gut-brain axis and cognitive control: A role for the vagus nerve. *Semin. Cell Dev. Biol.* **2024**, *156*, 201–209. [CrossRef]
67. Kasarello, K.; Cudnoch-Jedrzejewska, A.; Czarzasta, K. Communication of gut microbiota and brain via immune and neuroendocrine signaling. *Front. Microbiol.* **2023**, *14*, 1118529. [CrossRef]
68. Liu, Y.; Sanderson, D.; Mian, M.F.; McVey Neufeld, K.A.; Forsythe, P. Loss of vagal integrity disrupts immune components of the microbiota-gut-brain axis and inhibits the effect of Lactobacillus rhamnosus on behavior and the corticosterone stress response. *Neuropharmacology* **2021**, *195*, 108682. [CrossRef] [PubMed]
69. Rogers, A.P.; Mileto, S.J.; Lyras, D. Impact of enteric bacterial infections at and beyond the epithelial barrier. *Nat. Rev. Microbiol.* **2023**, *21*, 260–274. [CrossRef] [PubMed]
70. Gierynska, M.; Szulc-Dabrowska, L.; Struzik, J.; Mielcarska, M.B.; Gregorczyk-Zboroch, K.P. Integrity of the Intestinal Barrier: The Involvement of Epithelial Cells and Microbiota-A Mutual Relationship. *Animals* **2022**, *12*, 145. [CrossRef]
71. Brescia, C.; Audia, S.; Pugliano, A.; Scaglione, F.; Iuliano, R.; Trapasso, F.; Perrotti, N.; Chiarella, E.; Amato, R. Metabolic drives affecting Th17/Treg gene expression changes and differentiation: Impact on immune-microenvironment regulation. *APMIS* **2024**. [CrossRef]
72. de Candia, P.; Procaccini, C.; Russo, C.; Lepore, M.T.; Matarese, G. Regulatory T cells as metabolic sensors. *Immunity* **2022**, *55*, 1981–1992. [CrossRef]
73. Sasidharan Nair, V.; Heredia, M.; Samsom, J.; Huehn, J. Impact of gut microenvironment on epigenetic signatures of intestinal T helper cell subsets. *Immunol. Lett.* **2022**, *246*, 27–36. [CrossRef] [PubMed]
74. Shi, W.; Cassmann, T.J.; Bhagwate, A.V.; Hitosugi, T.; Ip, W.K.E. Lactic acid induces transcriptional repression of macrophage inflammatory response via histone acetylation. *Cell Rep.* **2024**, *43*, 113746. [CrossRef]
75. Jeffrey, M.P.; Saleem, L.; MacPherson, C.W.; Tompkins, T.A.; Clarke, S.T.; Green-Johnson, J.M. A Lacticaseibacillus rhamnosus secretome induces immunoregulatory transcriptional, functional and immunometabolic signatures in human THP-1 monocytes. *Sci. Rep.* **2024**, *14*, 8379. [CrossRef]
76. Jordan, C.K.I.; Brown, R.L.; Larkinson, M.L.Y.; Sequeira, R.P.; Edwards, A.M.; Clarke, T.B. Symbiotic Firmicutes establish mutualism with the host via innate tolerance and resistance to control systemic immunity. *Cell Host Microbe* **2023**, *31*, 1433–1449.e9. [CrossRef] [PubMed]

77. Nagahata, Y.; Masuda, K.; Nishimura, Y.; Ikawa, T.; Kawaoka, S.; Kitawaki, T.; Nannya, Y.; Ogawa, S.; Suga, H.; Satou, Y.; et al. Tracing the evolutionary history of blood cells to the unicellular ancestor of animals. *Blood* **2022**, *140*, 2611–2625. [CrossRef] [PubMed]
78. Storz, J.F.; Opazo, J.C.; Hoffmann, F.G. Gene duplication, genome duplication, and the functional diversification of vertebrate globins. *Mol. Phylogenet. Evol.* **2013**, *66*, 469–478. [CrossRef] [PubMed]
79. Mussini, G.; Dunn, F.S. Decline and fall of the Ediacarans: Late-Neoproterozoic extinctions and the rise of the modern biosphere. *Biol. Rev. Camb. Philos. Soc.* **2024**, *99*, 110–130. [CrossRef]
80. Evans, S.D.; Tu, C.; Rizzo, A.; Surprenant, R.L.; Boan, P.C.; McCandless, H.; Marshall, N.; Xiao, S.; Droser, M.L. Environmental drivers of the first major animal extinction across the Ediacaran White Sea-Nama transition. *Proc. Natl. Acad. Sci. USA* **2022**, *119*, e2207475119. [CrossRef]
81. Antell, G.T.; Saupe, E.E. Bottom-up controls, ecological revolutions and diversification in the oceans through time. *Curr. Biol.* **2021**, *31*, R1237–R1251. [CrossRef]
82. Mangano, M.G.; Buatois, L.A. The rise and early evolution of animals: Where do we stand from a trace-fossil perspective? *Interface Focus* **2020**, *10*, 20190103. [CrossRef] [PubMed]
83. Wood, R.; Liu, A.G.; Bowyer, F.; Wilby, P.R.; Dunn, F.S.; Kenchington, C.G.; Cuthill, J.F.H.; Mitchell, E.G.; Penny, A. Integrated records of environmental change and evolution challenge the Cambrian Explosion. *Nat. Ecol. Evol.* **2019**, *3*, 528–538, Erratum in *Nat. Ecol. Evol.* **2019**, *3*, 858.
84. Darroch, S.A.F.; Smith, E.F.; Laflamme, M.; Erwin, D.H. Ediacaran Extinction and Cambrian Explosion. *Trends Ecol. Evol.* **2018**, *33*, 653–663. [CrossRef]
85. Boem, F.; Greslehner, G.P.; Konsman, J.P.; Chiu, L. Minding the gut: Extending embodied cognition and perception to the gut complex. *Front. Neurosci.* **2023**, *17*, 1172783. [CrossRef] [PubMed]
86. Bateson, P. Adaptability and evolution. *Interface Focus* **2017**, *7*, 20160126. [CrossRef]
87. Tetlock, A.; Yost, C.K.; Stavrinides, J.; Manzon, R.G. Changes in the gut microbiome of the sea lamprey during metamorphosis. *Appl. Environ. Microbiol.* **2012**, *78*, 7638–7644. [CrossRef]
88. Mathai, P.P.; Byappanahalli, M.N.; Johnson, N.S.; Sadowsky, M.J. Gut Microbiota Associated with Different Sea Lamprey (*Petromyzon marinus*) Life Stages. *Front. Microbiol.* **2021**, *12*, 706683, Erratum in *Front. Microbiol.* **2021**, *12*, 807068. [CrossRef]
89. Salzer, J.L.; Zalc, B. Myelination. *Curr. Biol.* **2016**, *26*, R971–R975. [CrossRef] [PubMed]
90. Wyles, J.S.; Kunkel, J.G.; Wilson, A.C. Birds, behavior, and anatomical evolution. *Proc. Natl. Acad. Sci. USA* **1983**, *80*, 4394–4397. [CrossRef]
91. Zhang, Z.; Schäffer, A.A.; Miller, W.; Madden, T.L.; Lipman, D.J.; Koonin, E.V.; Altschul, S.F. Protein sequence similarity searches using patterns as seeds. *Nucleic Acids Res.* **1998**, *26*, 3986–3990. [CrossRef]
92. Gabler, F.; Nam, S.Z.; Till, S.; Mirdita, M.; Steinegger, M.; Soding, J.; Lupas, A.N.; Alva, V. Protein Sequence Analysis Using the MPI Bioinformatics Toolkit. *Curr. Protoc. Bioinform.* **2020**, *72*, e108. [CrossRef]
93. Larkin, M.A.; Blackshields, G.; Brown, N.P.; Chenna, R.; McGettigan, P.A.; McWilliam, H.; Valentin, F.; Wallace, I.M.; Wilm, A.; Lopez, R.; et al. Clustal W and Clustal X version 2.0. *Bioinformatics* **2007**, *23*, 2947–2948. [CrossRef] [PubMed]
94. Edgar, R.C. MUSCLE: Multiple sequence alignment with high accuracy and high throughput. *Nucleic Acids Res.* **2004**, *32*, 1792–1797. [CrossRef]
95. Gouy, M.; Guindon, S.; Gascuel, O. SeaView version 4: A multiplatform graphical user interface for sequence alignment and phylogenetic tree building. *Mol. Biol. Evol.* **2010**, *27*, 221–224. [CrossRef]
96. Shih, A.C.; Lee, D.T.; Peng, C.L.; Wu, Y.W. Phylo-mLogo: An interactive and hierarchical multiple-logo visualization tool for alignment of many sequences. *BMC Bioinform.* **2007**, *8*, 63. [CrossRef]
97. Van de Peer, Y.; De Wachter, R. TREECON for Windows: A software package for the construction and drawing of evolutionary trees for the Microsoft Windows environment. *Comput. Appl. Biosci.* **1994**, *10*, 569–570. [CrossRef]
98. Tamura, K.; Stecher, G.; Kumar, S. MEGA11: Molecular Evolutionary Genetics Analysis Version 11. *Mol. Biol. Evol.* **2021**, *38*, 3022–3027. [CrossRef]
99. Trifinopoulos, J.; Nguyen, L.T.; von Haeseler, A.; Minh, B.Q. W-IQ-TREE: A fast online phylogenetic tool for maximum likelihood analysis. *Nucleic Acids Res.* **2016**, *44*, W232–W235. [CrossRef]
100. Le, S.Q.; Lartillot, N.; Gascuel, O. Phylogenetic mixture models for proteins. *Philos. Trans. R Soc. Lond. B Biol. Sci.* **2008**, *363*, 3965–3976. [CrossRef]
101. Brandt, B.W.; Feenstra, K.A.; Heringa, J. Multi-Harmony: Detecting functional specificity from sequence alignment. *Nucleic Acids Res.* **2010**, *38*, W35–W40. [CrossRef]
102. Yariv, B.; Yariv, E.; Kessel, A.; Masrati, G.; Chorin, A.B.; Martz, E.; Mayrose, I.; Pupko, T.; Ben-Tal, N. Using evolutionary data to make sense of macromolecules with a "face-lifted" ConSurf. *Protein Sci.* **2023**, *32*, e4582. [CrossRef] [PubMed]
103. UniProt, C. UniProt: The Universal Protein Knowledgebase in 2023. *Nucleic Acids Res.* **2023**, *51*, D523–D531.
104. Drew, E.D.; Janes, R.W. 2StrucCompare: A webserver for visualizing small but noteworthy differences between protein tertiary structures through interrogation of the secondary structure content. *Nucleic Acids Res.* **2019**, *47*, W477–W481. [CrossRef]

105. Holm, L.; Laiho, A.; Törönen, P.; Salgado, M. DALI shines a light on remote homologs: One hundred discoveries. *Protein Sci.* **2023**, *32*, e4519. [CrossRef] [PubMed]
106. Li, Z.; Natarajan, P.; Ye, Y.; Hrabe, T.; Godzik, A. POSA: A user-driven, interactive multiple protein structure alignment server. *Nucleic Acids Res.* **2014**, *42*, W240–W245. [CrossRef] [PubMed]